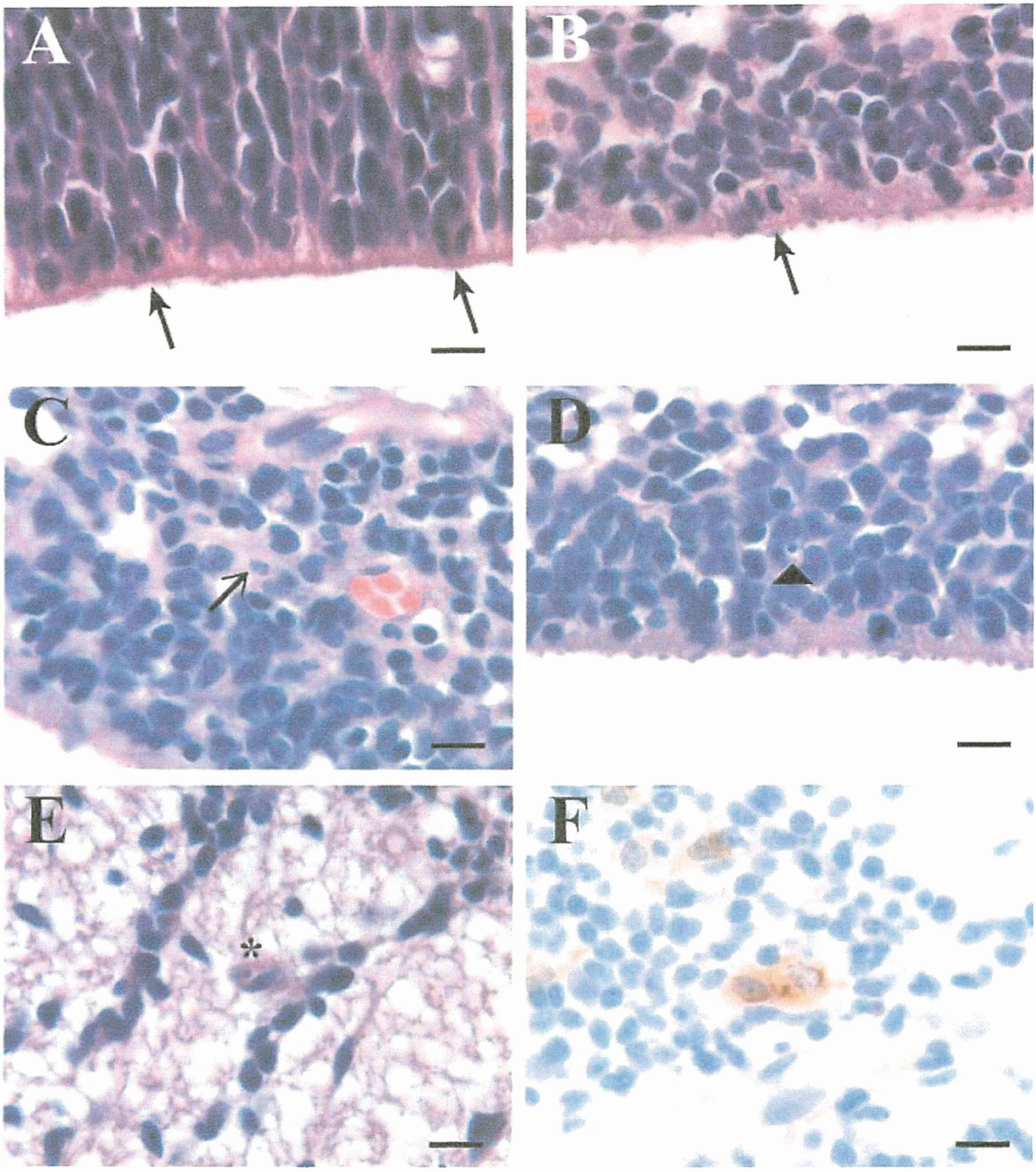

Figure 2. Ventricular zone at (A) E50 and (B through F) E80. (A, B) Mitoses (arrows) were noted in the bottom layer of the neuroepithelium. (C through E) Nuclear fragmentation (arrow), pyknosis (arrowhead), and macrophagic (asterisk) phagocytosis of cells with these characteristics were observed. (F) Cellular debris was phagocytized by Iba1-positive cells. (A through E) Hematoxylin and eosin stain; (F) Immnohistochemical staining of Iba1; bar, 10 µm.

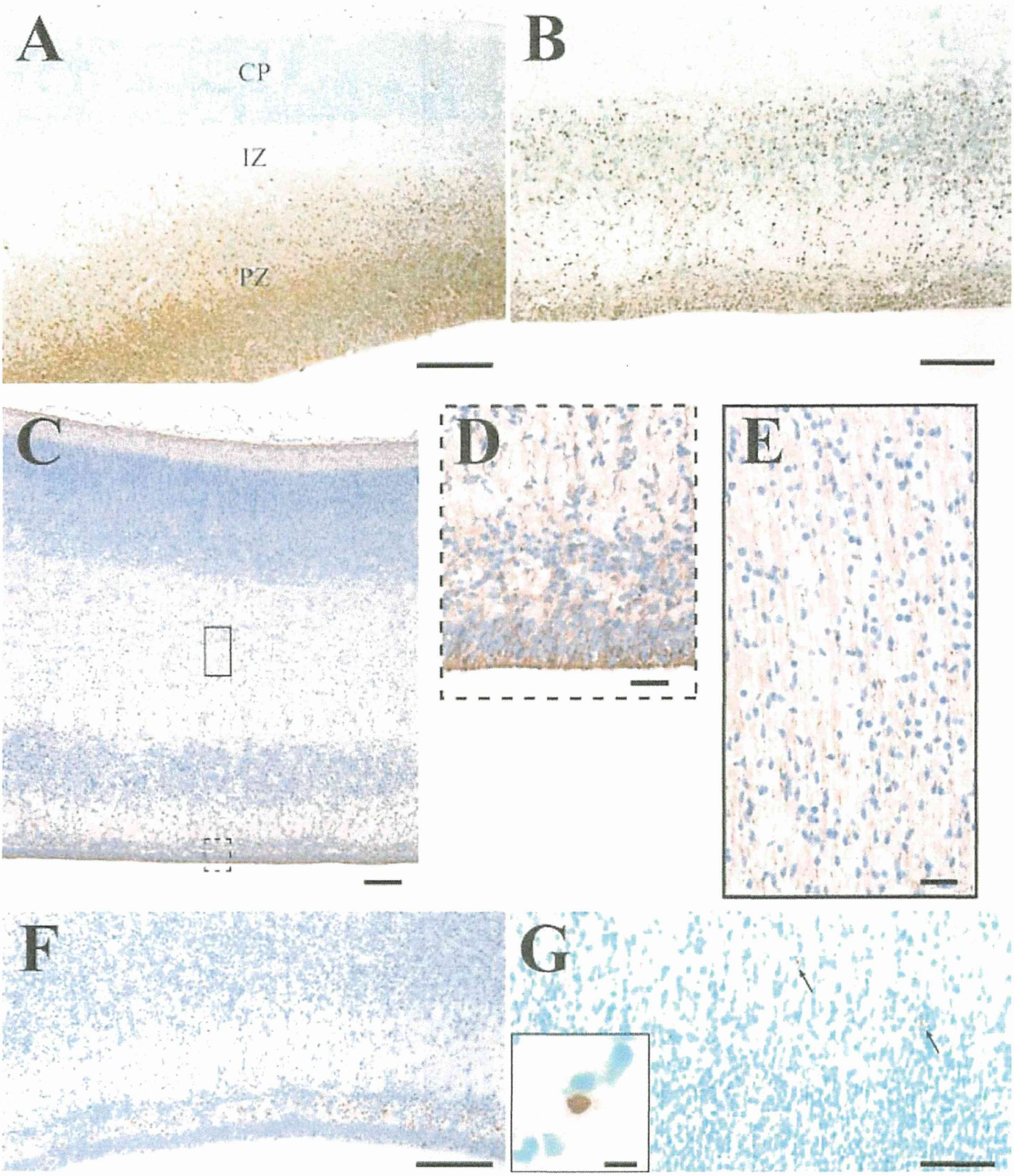

Figure 3. Immunohistochemical staining of PCNA at (A) E50 and (B) E80; methyl green counterstained. Most cells in the proliferative zone (PZ, ventricular and subventricular zones) were positive. (C through E) Immunohistochemical staining of GFAP and (F) Iba1 at E80; hematoxylin counterstained. (D) Neuroepithelium and (E) radial glial fibers that extend throughout the intermediate zone were positive for GFAP, whereas (F) Iba1-positive cells were localized in the ventricular zone. (G) TUNEL staining at E50; methyl green counterstained. TUNEL-positive cells (arrows) were sparsely distributed in the ventricular zone. Bar: 100 μm (A through C, F, and G); 25 μm (D, E); 2 μm (inset of G).

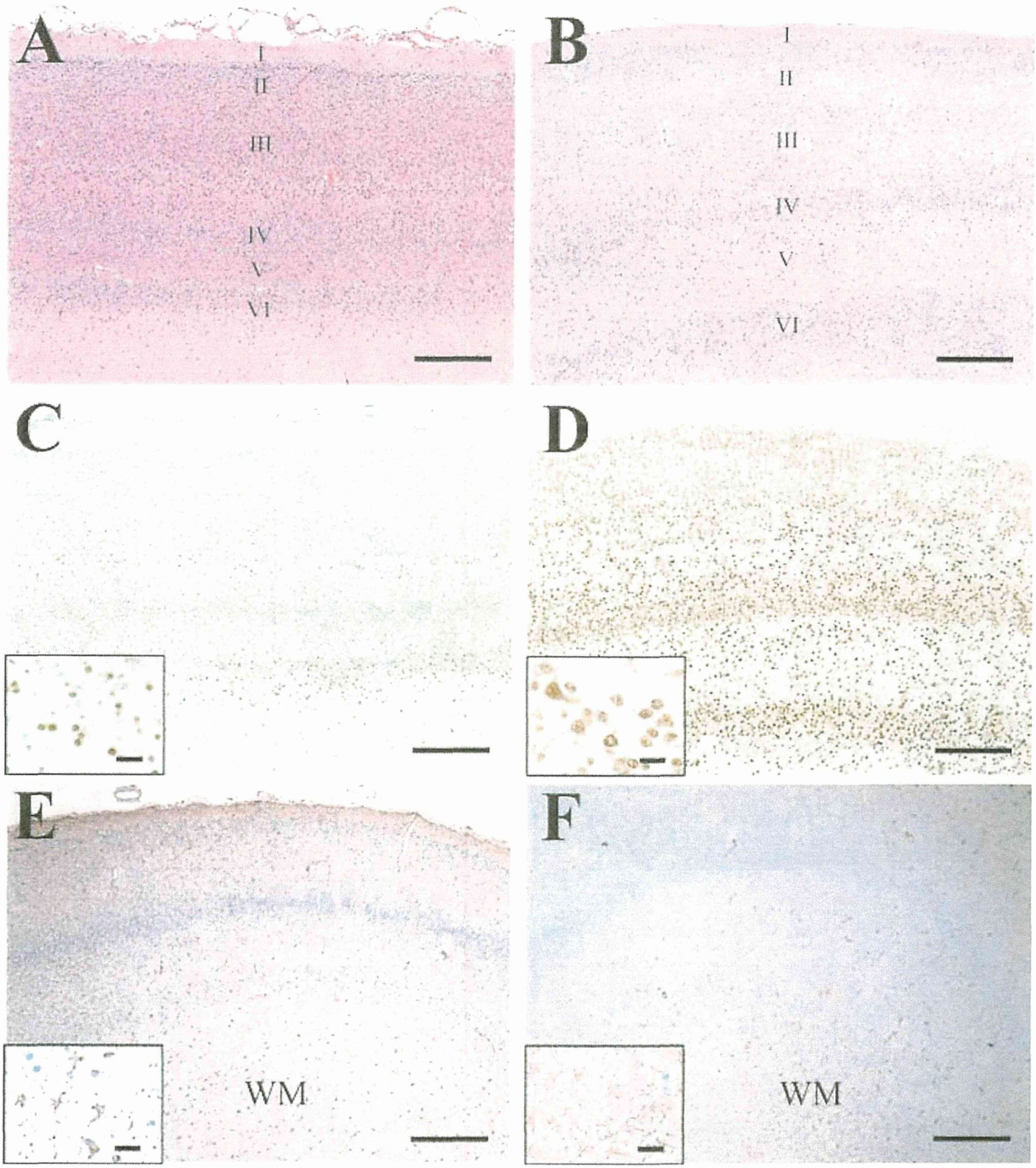

Figure 4. Hematoxylin and eosin staining of the cerebral cortex at (A) E120 and (B) E150. The cerebral cortex consisted of 6 layers. (C) Immunohistochemical staining of NeuN; methyl green counterstained. Most cells in all layers, except for layer I-II, were strongly positive. (C, inset) Higher magnification of layer III shows that the nuclei of cells with scant cytoplasm were positive. (D) Almost all cells of the cerebral cortex were NeuN-positive, with particularly strong staining both the nucleus and cytoplasm of cells with processes in layer III (inset). Immunohistochemical staining of GFAP at (E) E120 and (F) E150; hematoxylin counterstained. Many cells with short processes mainly in the white matter (WM, inset) were strongly positive. Radial glial fibers observed at E80 were not present (inset). Bar: 200 µm (E); 100 µm (A through D); 50 µm (F); 20 µm (inset of C through F).

and spatial patterns between E50 and E80. TUNEL-positive cells in the current study were fewer (0 to 2.1 per 1000 cells) than those reported for rodents,[3,4] humans,[26,31] and rhesus monkeys.[13] This result may be explained by the fact that apoptotic cells are removed rapidly, in about 2 to 3 h.[34]

Apoptosis is thought to induce timely disappearance of various structures during brain development. For example, in humans, TUNEL-positive cells are detected in the marginal zone beginning during the second trimester of pregnancy. The numbers of apoptotic cells increase until the disappearance of the subpial granular layer (23 to 30 GW) and significantly decrease overall in layer I after 30 GW.[33] However, in the current study, the TUNEL method failed to detect any apoptotic cells in the cerebral cortex after E120. Therefore, apoptosis-induced temporal disappearance of brain structure may not occur after this point in fetal cynomolgus macaques. In addition, we noted very few apoptotic cells at or before E80, when the proliferation and migration of neural cells were active, indicating that apoptosis plays an important role in targeting undifferentiated or irregularly differentiated cells.[3]

To investigate the involvement of microglia in the removal of apoptotic cells, we performed immunohistochemistry using antiIba1 antibody. Iba1 is a 17-kDa EF-hand protein that is specifically expressed in macrophages and microglia and is upregulated during the activation of these cells.[15] In the current study, Iba1 immunoreactivity was detected during gestation, but it was not temporally correlated with apoptotic cells, a finding that is inconsistent with previous reports from rat and human fetal brains.[10,26] Although we noted no temporal correlation between microglial accumulation and apoptosis, other studies report the aggregation of microglial cells around the neuroepithelium in the telencephalic wall that contain phagocytized pyknotic nuclei, suggesting the involvement of these microglia in cell death.[2,24] In addition, the present study revealed the presence of Iba1-positive cells (that is, microglial cells) that had phagocytized cellular debris in proliferative zone at E80. As mentioned earlier, microglia may be associated with the removal of dead cells in the developing brain, because characteristic features such as nuclear fragmentation were present in the proliferative zone at E80. A characteristic finding in the present study was the aggregation of microglia localized around the ventricular zone at E80. This distribution at E80 corresponds to that of humans between 12 to 24 GW, which is equivalent to E50 to E80.[28] The aggregated microglial cells may be involved with the disappearance of temporary structures in the developing brain, such as the subventricular and subplate zones, because the subventricular zone declines dramatically between mid- and late gestation.[5] Alternatively, microglial cells may enter the CNS from within or around the ventricular and subventricular zones during CNS development. In either case, the cause of aggregation remains unclear, and further studies are needed to define the functional roles of microglia during brain development.

To investigate the differentiation of neuronal cells, we performed immunohistochemistry using antiNeuN antibody. NeuN is a transcriptional factor that is expressed in the nucleus and cytoplasm of neurons after postmitotic precursor cells start to differentiate into mature cells cytologically and morphologically.[21] Moreover, immature neuronal cells that do not have mature function are negative for NeuN. Therefore, NeuN is a useful marker of the developing CNS because it labels the nucleus rather than the cytoplasm and can be detected even in cells with scant cytoplasm.[30,36] In the current study, NeuN immunoreactivity was not detected at E50 or E80, whereas most cells in the cerebral cortex were positive at E120 and E150. In humans, NeuN is expressed in layers IV to VI at 20 GW,[30] although some reports show that expression of NeuN is not revealed at 26 GW.[1] The visual cortex during E70 to E105 in monkeys is histologically similar to that during 18 to 30 GW in humans,[18] and data obtained from the present study were consistent with those in humans. In addition, laminar formation of the cerebral cortex is induced during approximately this same time frame.[18] Therefore, these combined data indicate that functional neuronal differentiation starts around the time of laminar formation of the cerebral cortex.

Radial glial cells are important in guiding the migration of immature neurons, which differentiate into astrocytes after completing migration.[25] Some reports show that they also differentiate into neurons.[20,23] GFAP immunohistochemistry in the current study revealed the existence of glial cells with varied morphology. At E50 and E80, the neuroepithelium was positive for GFAP. Radial glial fibers elongating vertically from the ventricle to pia mater between E50 and E80 were strongly positive, but the numbers of radial glial cells had decreased by E120, and cells with short processes, such as mature astrocytes, increased. These results are reasonably consistent with a previous report in rhesus monkeys.[19] Some reports in humans show that radial glial cells decrease beginning in the second trimester, and mature astrocytes appear at 30 GW.[9,14,33] These data closely reflect the findings of the present study.

In conclusion, the cerebrum of fetal cynomolgus monkeys at E50 and E80 contained many mitoses and PCNA-positive cells, as well as radial glial fibers that help in cell migration. Apoptosis, phagocytosis, and aggregated microglia were present. These results suggest that proliferation, migration, and cell death of neural cells are predominant until mid-gestation (E80). At E120 and E150, the cerebral cortex showed a decrease in the number of proliferating cells, the disappearance of radial glial fibers, and the appearance of mature astrocytes and mature neurons. These results suggest that differentiation or maturation of neural cells starts after the mid-gestational period in the cynomolgus monkey fetus. These findings are relevant to the timing of neurologic developmental events in nonhuman primates and, because of the physiologic similarities of humans to nonhuman primates, are pertinent to the use of nonhuman primates for neurodevelopmental toxicologic research

Acknowledgments

This work was supported by the Department of Veterinary Pathology (Nippon Veterinary and Life Science University). We thank the feeding and experimental staff in Shin Nippon Biomedical Laboratories. This work was supported in part by Grants-in-Aid for Scientific Research from the Japan Society for the Promotion of Science.

References

1. **Anlar B, Atilla P, Cakar N, Tombakoglu M, Bulun A.** 2003. Apoptosis in the developing human brain: a preliminary study of the frontal region. Early Hum Dev 71:53–60.
2. **Ashwell K.** 1991. The distribution of microglia and cell death in the fetal rat forebrain. Brain Res Dev Brain Res 58:1–12.
3. **Blaschke AJ, Staley K, Chun J.** 1996. Widespread programmed cell death in proliferative and postmitotic regions of the fetal cerebral cortex. Development 122:1165–1174.
4. **Blaschke AJ, Weiner JA, Chun J.** 1998. Programmed cell death is a universal feature of embryonic and postnatal neuroproliferative

regions throughout the central nervous system. J Comp Neurol 396:39–50.
5. Chan WY, Lorke DE, Tiu SC, Yew DT. 2002. Proliferation and apoptosis in the developing human neocortex. Anat Rec 267:261–276.
6. Chan WY, Yew DT. 1998. Apoptosis and Bcl2 oncoprotein expression in the human fetal central nervous system. Anat Rec 252:165–175.
7. Cowan WM, Fawcett JW, O'Leary DD, Stanfield BB. 1984. Regressive events in neurogenesis. Science 225:1258–1265.
8. Dalmau I, Vela JM, González B, Finsen B, Castellano B. 2003. Dynamics of microglia in the developing rat brain. J Comp Neurol 458:144–157.
9. deAzevedo LC, Fallet C, Moura-Neto V, Daumas-Duport C, Hedin-Pereira C, Lent R. 2003. Cortical radial glial cells in human fetuses: depth-correlated transformation into astrocytes. J Neurobiol 55:288–298.
10. Ferrer I, Serrano T, Soriano E. 1990. Naturally occurring cell death in the subicular complex and hippocampus in the rat during development. Neurosci Res 8:60–66.
11. Gavrieli Y, Sherman Y, Ben-Sasson SA. 1992. Identification of programmed cell death in situ via specific labeling of nuclear DNA fragmentation. J Cell Biol 119:493–501.
12. Giorno R. 1984. A comparison of two immunoperoxidase staining methods based on the avidin-biotin interaction. Diagn Immunol 2:161–166.
13. He N, Song ZM, Lidow MS. 1999. Cocaine induces cell death within the primate fetal cerebral wall. Neuropathol Appl Neurobiol 25:504–512.
14. Honig LS, Herrmann K, Shatz CJ. 1996. Developmental changes revealed by immunohistochemical markers in human cerebral cortex. Cereb Cortex 6:794–806.
15. Imai Y, Ibata I, Ito D, Ohsawa K, Kohsaka S. 1996. A novel gene (*iba1*) in the major histocompatibility complex class III region encoding an EF hand protein expressed in a monocytic lineage. Biochem Biophys Res Commun 224:855–862.
16. Institute for Laboratory Animal Research. 1996. Animal environment, housing, and management, p 21–55. In: Guide for the care and use of laboratory animals, 7th ed. Washington (DC): National Academies Press.
17. Kendler A, Golden JA. 1996. Progenitor cell proliferation outside the ventricular and subventricular zones during human brain development. J Neuropathol Exp Neurol 55:1253–1258.
18. Kostovic I, Rakic P. 1990. Developmental history of the transient subplate zone in the visual and somatosensory cortex of the macaque monkey and human brain. J Comp Neurol 297:441–470.
19. Levitt P, Rakic P. 1980. Immunoperoxidase localization of glial fibrillary acidic protein in radial glial cells and astrocytes of the developing rhesus monkey brain. J Comp Neurol 193:815–840.
20. Malatesta P, Hartfuss E, Götz M. 2000. Isolation of radial glial cells by fluorescent-activated cell sorting reveals a neuronal lineage. Development 127:5253–5263.
21. Mullen RJ, Buck CR, Smith AM. 1992. NeuN, a neuronal specific nuclear protein in vertebrates. Development 116:201–211.
22. Møllgård K, Schumacher U. 1993. Immunohistochemical assessment of cellular proliferation in the developing human CNS using formalin-fixed paraffin-embedded material. J Neurosci Methods 46:191–196.
23. Noctor SC, Flint AC, Weissman TA, Dammerman RS, Kriegstein AR. 2001. Neurons derived from radial glial cells establish radial units in neocortex. Nature 409:714–720.
24. Perry VH, Hume DA, Gordon S. 1985. Immunohistochemical localization of macrophages and microglia in the adult and developing mouse brain. Neuroscience 15:313–326.
25. Rakic P. 1995. Corticogenesis in human and nonhuman primates, p 127–145. In: Gazzaniga MS, editor. Cognitive neuroscience. Boston (MA): MIT Press.
26. Rakic S, Zecevic N. 2000. Programmed cell death in the developing human telencephalon. Eur J Neurosci 12:2721–2734.
27. Rezaie P. 2003. Microglia in the human nervous system during development. Neuroembryology Aging 2:18–31.
28. Rezaie P, Dean A, Male D, Ulfig N. 2005. Microglia in the cerebral wall of the human telencephalon at second trimester. Cereb Cortex 15:938–949.
29. Sabattini E, Bisgaard K, Ascani S, Poggi S, Piccioli M, Ceccarelli C, Pieri F, Fraternali-Orcioni G, Pileri SA. 1998. The EnVision++ system: a new immunohistochemical method for diagnostics and research. Critical comparison with the APAAP, ChemMate, CSA, LABC, and SABC techniques. J Clin Pathol 51:506–511.
30. Sarnat HB, Nochlin D, Born DE. 1998. Neuronal nuclear antigen (NeuN): a marker of neuronal maturation in early human fetal nervous system. Brain Dev 20:88–94.
31. Simonati A, Rosso T, Rizzuto N. 1997. DNA fragmentation in normal development of the human central nervous system: a morphological study during corticogenesis. Neuropathol Appl Neurobiol 23:203–211.
32. Simonati A, Tosati C, Rosso T, Piazzola E, Rizzuto N. 1999. Cell proliferation and death: morphological evidence during corticogenesis in the developing human brain. Microsc Res Tech 45:341–352.
33. Spreafico R, Arcelli P, Frassoni C, Canetti P, Giaccone G, Rizzuti T, Mastrangelo M, Bentivoglio M. 1999. Development of layer I of the human cerebral cortex after midgestation: architectonic findings, immunocytochemical identification of neurons and glia, and in situ labeling of apoptotic cells. J Comp Neurol 410:126–142.
34. Thomaidou D, Mione MC, Cavanagh JF, Parnavelas JG. 1997. Apoptosis and its relation to the cell cycle in the developing cerebral cortex. J Neurosci 17:1075–1085.
35. Voiculescu B, Nat R, Lin E, Iosef C. 2000. Apoptosis in human embryo development: 1. Cerebral cortex. J Cell Mol Med 4:284–288.
36. Wolf HK, Buslei R, Schmidt-Kastner R, Schmidt-Kastner PK, Pietsch T, Wiestler OD, Blümcke I. 1996. NeuN: a useful neuronal marker for diagnostic histopathology. J Histochem Cytochem 44:1167–1171.

RESEARCH

Effects of ubiquitin C-terminal hydrolase L1 deficiency on mouse ova

Sayaka Koyanagi[1], Hiroko Hamasaki[1], Satoshi Sekiguchi[1], Kenshiro Hara[2], Yoshiyuki Ishii[1], Shigeru Kyuwa[1] and Yasuhiro Yoshikawa[1,3]

Department of [1]Biomedical Science and [2]Veterinary Anatomy, Graduate School of Agricultural and Life Sciences, The University of Tokyo, Yayoi 1-1-1, Bunkyo-ku, Tokyo 113-8657, Japan and [3]Laboratory of Zoonoses, School of Veterinary Medicine, Kitasato University, Towada, Aomori 034-8628, Japan

Correspondence should be addressed to S Kyuwa; Email: akyuwa@mail.ecc.u-tokyo.ac.jp

K Hara is now at Division of Germ Cell Biology, National Institute for Basic Biology, National Institutes for Natural Sciences, Okazaki 444-8787, Japan

Abstract

Maternal proteins are rapidly degraded by the ubiquitin–proteasome system during oocyte maturation in mice. Ubiquitin C-terminal hydrolase L1 (UCHL1) is highly and specifically expressed in mouse ova and is involved in the polyspermy block. However, the role of UCHL1 in the underlying mechanism of polyspermy block is poorly understood. To address this issue, we performed a comprehensive proteomic analysis to identify maternal proteins that were relevant to the role of UCHL1 in mouse ova using UCHL1-deficient *gad*. Furthermore, we assessed morphological features in *gad* mouse ova using transmission electron microscopy. NACHT, LRR, and PYD domain-containing (NALP) family proteins and endoplasmic reticulum (ER) chaperones were identified by proteomic analysis. We also found that the 'maternal antigen that embryos require' (NLRP5 (MATER)) protein level increased significantly in *gad* mouse ova compared with that in wild-type mice. In an ultrastructural study, *gad* mouse ova contained less ER in the cortex than in wild-type mice. These results provide new insights into the role of UCHL1 in the mechanism of polyspermy block in mouse ova.

Reproduction (2012) 143 271–279

Introduction

Maternal proteins are synthesized and degraded dynamically during oocyte maturation. Intracellular protein degradation plays important roles in modulating the levels of specific proteins and eliminating damaged proteins to achieve fertilization and early embryo development. The ubiquitin–proteasome system is a major pathway for selective intracellular protein degradation in ova. Ubiquitination of proteins is recognized to target proteins for degradation by proteasomes and for internalization into the lysosomal system. Deubiquitinating enzymes (DUBs) regulate ubiquitination and regenerate free ubiquitin after proteins have been targeted to the proteasome or lysosome.

While other DUB members are ubiquitously expressed, ubiquitin C-terminal hydrolase L1 (UCHL1), one of the DUBs, is selectively expressed in neurons and germ cells (Wilson *et al.* 1988, Wilkinson *et al.* 1989). Recent studies suggest that UCHL1 associates with monoubiquitin and prolongs the ubiquitin half-life in neurons (Osaka *et al.* 2003) and that UCHL1 regulates apoptosis in testicular germ cells (Kwon *et al.* 2004, 2005). However, the role of UCHL1 in ova is largely unknown. We previously reported that UCHL1 is exclusively localized on the plasma membrane of mouse ova and plays an important role in the polyspermy block (Sekiguchi *et al.* 2006). Polyspermic fertilization refers to the penetration of ova by two or more spermatozoa, resulting in the developmental failure of the zygote (Sun 2003). It is necessary to block polyspermy for successful fertilization. At the time of fertilization, polyspermy is prevented primarily by the zona pellucida (ZP) block (also known as the zona reaction) following cortical granule exocytosis (CGE) in mammalian ova (Hatanaka *et al.* 1992). Susor *et al.* (2010) showed that UCHL1 regulates CG reorganization and contributes to the ZP block using UCHL1 inhibitors. In contrast, 'gracile axonal dystrophy' (*gad*) female mice, which are autosomal recessive, spontaneous mutants carrying an intragenic deletion of the gene encoding UCHL1, show a significantly increased *in vitro* polyspermy rate and a decrease in litter size, even though *gad* mouse ova undergo a normal zona reaction (Saigoh *et al.* 1999, Sekiguchi *et al.* 2006). Thus, the role of

ISSN 1470–1626 (paper) 1741–7899 (online)

DOI: 10.1530/REP-11-0128
Online version via www.reproduction-online.org

UCHL1 in the mechanism of inhibiting polyspermy in mouse ova remains unclear.

To address these issues, we sought to identify the difference in protein expression induced by *Uchl1* deletion, based on a comprehensive proteomic analysis using *gad* mice, and identified maternal-specific proteins and endoplasmic reticulum (ER) chaperones that were relevant to the role of UCHL1 in mouse ova. Further, we observed morphological changes in *gad* mouse ova using transmission electron microscopy (TEM). These findings have important implications for understanding the role of UCHL1 in mouse ova.

Results

Normal expression of F-actin and cofilin in gad *mouse ova*

F-actin is necessary for CGE, changes membrane structure at fertilization, and consequently blocks polyspermy of ova (Tsaadon *et al.* 2006). We investigated the protein expression and localization of F-actin and its depolymerizing factor, cofilin, in wild-type and *gad* mouse ova (Fig. 1). Cofilin belongs to a family of F-actin depolymerizing factors that are highly conserved throughout the animal kingdom. The cofilin protein severs actin filaments and promotes actin dynamics by accelerating the treadmilling of actin filaments, a process in which monomers are removed from the pointed end of the filaments and are added to the barbed end (Carlier *et al.* 1997). However, no difference in the protein level or localization was observed between the wild-type and *gad* mouse ova.

Identification of differentially expressed ovum proteins by proteomic analysis

A typical proteomic analysis involves three fundamental steps: 1) proteins of a complex mixture are separated and digested into peptide units, 2) peptide masses are determined using mass spectroscopy, and 3) proteins are identified by searching databases for matching peptides (Kirkpatrick *et al.* 2005). In this study, liquid chromatography–tandem mass spectrometry (LC–MS/MS) was used. The list of proteins that were downregulated or upregulated with statistical significance (one-sided P value <0.025) in *gad* mouse ova is presented in Table 1. ZP1 is a component of the ZP, consisting of three glycoproteins (ZP1, ZP2, and ZP3), and cross-links ZP2 and ZP3 (Wassarman & Litscher 2008). TLE6 belongs to the *Groucho/Tle* superfamily of transcriptional corepressors that plays critical roles in a range of developmental processes (Bajoghli 2007, Buscarlet & Stifani 2007). ENPL, HSPA5 (GRP78), and CALR are ER chaperones and regulators of the unfolded protein response (UPR) in the ER (Qiu & Michalak 2009, Eletto *et al.* 2010, Pfaffenbach & Lee 2011). NLRP14 (NALP14) is a member of the NALP family, which consists of 14 members. The family members have quite similar domain structures and expression during oogenesis and embryogenesis. Thus, they are assumed to have common functions during oocyte maturation and early embryo development (Zhang *et al.* 2008). However, at present, there is little information about NLRP14 and its function remains to be determined. In contrast, NLRP5 (NALP5), one of the NALP family members, has been well studied. Furthermore, the NLRP5 protein has many characteristics in common with UCHL1. Their expression levels and subcellular localization are strongly correlated throughout oogenesis and embryogenesis (Li *et al.* 2008, Ohsugi *et al.* 2008). NLRP5 localizes in the subcortex of ova and is excluded from the region of cell–cell contact at the two-cell stage. Correspondingly, UCHL1 shows the similar expression pattern in the ovum and at the two-cell stage (Fig. 2). Thus, in this study, we focused on the NLRP5 protein for its interesting similarities to UCHL1.

Expression and localization of the NLRP5 protein in mouse ova

We conducted a western blot analysis to confirm the expression levels of the NLRP5 protein in ova obtained from *gad* mice with those from wild-type mice. Levels of NLRP5 in *gad* mouse ova were significantly higher than those in wild-type mouse ova ($P=0.022$; Fig. 3A and B). Furthermore, to assess the relationship between UCHL1 and NLRP5, we analyzed their localization in wild-type and *gad* mouse ova. The two proteins colocalized on the plasma membrane and in the subcortex of wild-type

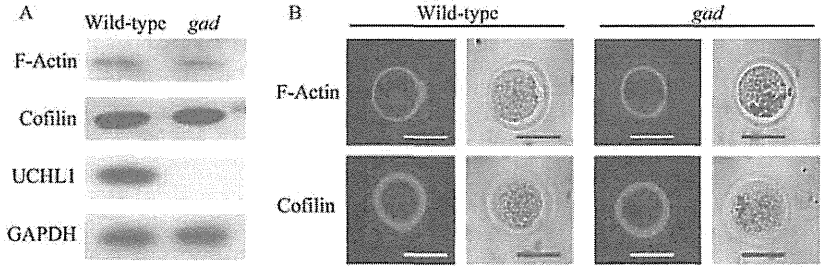

Figure 1 Expression and localization of F-actin and cofilin proteins in mouse ova. (A) Western blot analysis of F-actin, cofilin, ubiquitin C-terminal hydrolase L1 (UCHL1), and GAPDH in ova from wild-type ($n=6$) and *gad* ($n=7$) mice. No significant difference was observed in the F-actin and cofilin protein levels. UCHL1 was not detected in *gad* mouse ova. (B) F-actin and cofilin immunoreactivity are seen on the plasma membrane of ova from wild-type and *gad* mice. Bars, 50 μm.

Table 1 Differentially expressed oocyte proteins in wild-type and *gad* mice by liquid chromatography–mass spectrometry analysis.

Identified proteins	Molecular weight (kDa)	Expression level (wild-type (wt) vs *gad*)	*P* value (one-sided)
Zona pellucida sperm-binding protein 1 precursor (ZP1)	69	wt<*gad*	0.022
Transducin-like enhancer protein 6 (TLE6)	65	wt<*gad*	0.025
Endoplasmin precursor (ENPL)	92	wt<*gad*	0.022
78 kDa glucose-regulated protein precursor (HSPA5)	72	wt<*gad*	0.023
Calreticulin precursor (CALR)	48	wt<*gad*	0.002
NACHT, LRR, and PYD domain-containing protein 14 (NLRP14)	113	wt<*gad*	0.023
Ubiquitin C-terminal hydrolase L1 (UCHL1)	25	wt>*gad*	0.002

mouse ova (Fig. 4). However, the localization of NLRP5 in *gad* mouse ova was not different from that in wild-type mice (Fig. 4).

Ultrastructural observations of gad mouse ova

To assess whether *gad* mouse ova have a morphologically normal cortex structure, we analyzed them ultrastructurally by TEM (Fig. 5). Although basic structures such as CGs, microvilli, and cytoplasmic lattices (CPLs) were observed in both wild-type and *gad* mouse ova, there were no obvious structures that can be identified with ER cluster in the cortex of *gad* mouse ova.

Discussion

This study provided important findings on the role of UCHL1 in the mechanism of polyspermy block in mouse ova. It is necessary to block polyspermy for successful fertilization, which primarily involves a ZP block in mammalian ova. The ZP block comprises CGE and modification of the ZP so that the plasma membrane cannot support sperm binding by the enzymes released from CGs. F-actin regulates the movement of CGs toward the cortex during oocyte maturation and anchors them at the cortex (Connors *et al.* 1998). F-actin depolymerization occurs at CGE, and the protein level of F-actin decreases after fertilization (Eliyahu *et al.* 2005). We observed that the F-actin and cofilin protein expression levels and distribution on the plasma membrane were similar between the wild-type and *gad* mouse ova. We also found decreased F-actin protein levels, but no significant difference between the wild-type and *gad* mouse zygotes was observed after fertilization (data not shown). These results confirm our results of the CGE and ZP reaction in *gad* mouse ova (Sekiguchi *et al.* 2006). However, each protein is recognized differentially according to various post-translational modifications, such as phosphorylation and ubiquitination (Kirkpatrick *et al.* 2005). In fact, cofilin proteins are thought to be regulated through phosphorylation and activated by dephosphorylation at the serine residue (Meberg & Bamburg 2000). Thus, these findings suggest that cofilin proteins in *gad* mouse oocytes might be degenerated or modified differently from those in wild-type ova. Further experiments are needed to confirm this.

We then conducted a comprehensive proteomic analysis to identify any UCHL1-related proteins using *gad* mouse ova and identified NALP family proteins. The NALP family has 14 members with similar domain structures, and thus members are assumed to have common functions (Zhang *et al.* 2008). Almost all NALP family genes are expressed during oogenesis and embryogenesis (Zhang *et al.* 2008). We then focused on NLRP5 and confirmed protein expression and localization in wild-type and *gad* mice. The specificity and quantification of the LC–MS/MS method are greater than or equal to immunoassays including western blot and immunocytochemical staining. However, the high specificity enables us to reduce false-positive, but, on the other hand, it also reduces sensitivity (Kruse *et al.* 2008, Krone *et al.* 2010). Hence, this is the reason why NLRP5 was not detected by LC–MS/MS analysis in this study. The NLRP5 protein has many characteristics in common with UCHL1 (Sekiguchi *et al.* 2006, Ohsugi *et al.* 2008). First, UCHL1 and NLRP5 protein expression persist from immature oocytes in a primary follicle until the blastocyst stage.

Secondly, UCHL1 and NLRP5 may play an important role in oocyte maturation or embryogenesis because both *gad* and NLRP5-deficient females attain normal sexual maturity with intact ovarian folliculogenesis and the ability to ovulate fertilizable ova, but they have severe defects in reproduction. Thirdly, the most interesting analogy is the subcellular localization; neither protein is detected in the region of contact between the blastomeres, and they are restricted to the periphery through embryogenesis. This shared and unique expression pattern appears to indicate an interaction, such as regulation of NLRP5 protein levels by the ubiquitin–proteasome system including UCHL1. In fact, we found a significant increase in NLRP5 protein levels in *gad* mice with localization on the plasma membrane and subcortex.

The NLRP5 protein was identified abundantly and is an excellent candidate for a maternal-effect protein for the maturation and ovulation of ova (Zhang *et al.* 2009). The NLRP5 protein and transcript accumulate during oogenesis, and the transcript is almost completely degraded during meiotic maturation (Su *et al.* 2007, Li *et al.* 2008, Ohsugi *et al.* 2008). In contrast to the dramatic decrease in the transcript, the protein remains largely unchanged until the early blastocyst stage, suggesting that the protein level is properly regulated by degradation for the maintenance and control of

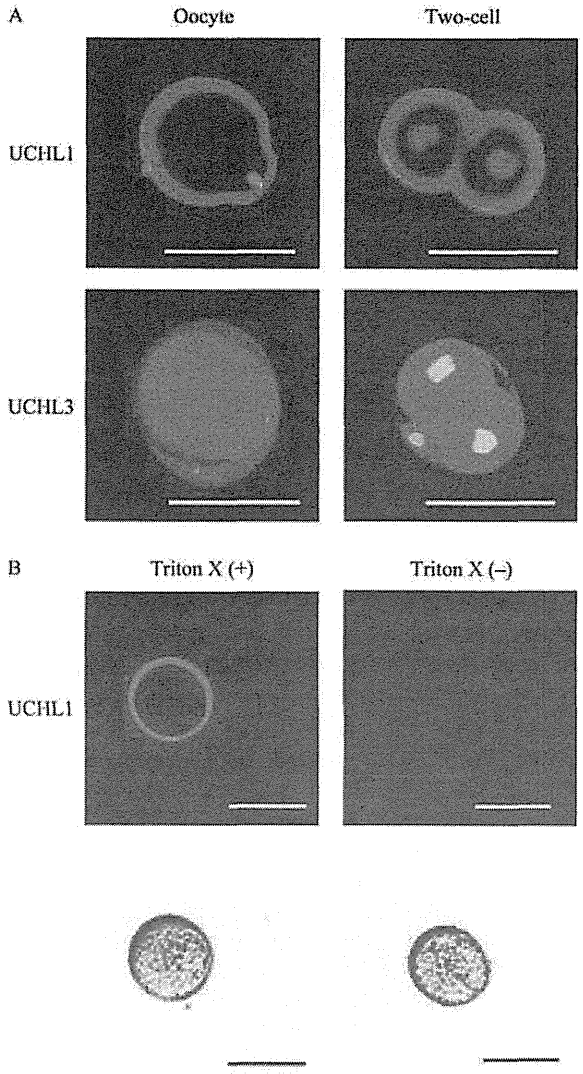

Figure 2 Localization of ubiquitin C-terminal hydrolase L1 (UCHL1) and UCHL3 in wild-type mouse ova. (A) UCHL1 immunoreactivity is seen on the plasma membrane of the ovum and at the two-cell stage. On the other hand, UCHL3, one of the DUBs, is seen in the cytoplasm of the ovum and at the two-cell stage. (B) While UCHL1 immunoreactivity is seen on the plasma membrane when treated with Triton X-100, it is not seen in the ova when not treated with Triton X-100. Bars, 50 μm.

maturation, fertilization, and early embryo development. Degradation of maternal proteins and transcripts is carried out rapidly in many organisms and plays a critical role in oocyte maturation. Most protein degradation is regulated by the ubiquitin–proteasome system and any impairment in degradation results in the failure of oocyte maturation (DeRenzo & Seydoux 2004, Huo *et al.* 2004, Ryu *et al.* 2008, Beall *et al.* 2010). UCHL1 is essential for maintaining the ubiquitin–proteasome system and is abundantly expressed in mouse ova (Sekiguchi *et al.* 2006). Similarly, previous studies have identified UCHL1 as a maternal protein necessary for oocyte maturation (Ellederova *et al.* 2004, Massicotte *et al.* 2006, Susor *et al.* 2007). Thus, a logical potential conclusion would be that the NLRP5 protein level is potentially regulated by the ubiquitin–proteasome system for oocyte maturation. In fact, ubiquitin mRNA levels are upregulated when the NLRP5 protein decreases during oogenesis and embryogenesis (Robert *et al.* 2002, Pennetier *et al.* 2006, Ohsugi *et al.* 2008). Furthermore, a UCHL1 inhibitor prevents germinal vesicle (GV) breakdown and the metaphase I–anaphase transition in porcine oocytes by downregulating the ubiquitin–proteasome system (Susor *et al.* 2007). Thus, excess NLRP5 protein resulting from downregulating the ubiquitin–proteasome system prevents complete oocyte maturation. Recent studies have reported that NLRP5 forms a subcortical maternal complex (SCMC) with maternally encoded proteins, an oocyte-specific binding protein of NLRP5 (FILIA), 'a factor located in oocytes permitting embryonic development' (FLOPED), and a putative transcriptional corepressor (TLE6; Li *et al.* 2008, Ohsugi *et al.* 2008). Considering that TLE6 was significantly upregulated in *gad* ova (Table 1), it seems likely that SCMC of *gad* mouse ova had difficulty in regulating the component balance. Thus, further research is required to understand the relationship between maternal proteins and UCHL1 in mouse ova. Taken together, we hypothesized that *gad* mouse ova polyspermy is caused by oocyte maturation failure (Fig. 6).

To test this, we investigated whether *gad* mouse ova showed morphological characteristics of immaturity using TEM. As expected, the CG of *gad* mouse ova localized normally. This result provides further support for our previous work (Sekiguchi *et al.* 2006). Recent reports have shown that NLRP5 also localizes to the CPLs, and *Mater*$^{tm/tm}$ mouse ova lack CPLs (Kim *et al.* 2010, Tashiro *et al.* 2010). Unlike *Nlrp5* hypomorphic mice, *gad* mouse ova containing excess NLRP5 protein showed normal CPLs. Interestingly, there were no obvious structures that can be identified with ER cluster in the cortex of *gad* mouse ova. The ER is a multifunctional and highly dynamic organelle involved in lipid and protein synthesis and is a major internal store of calcium ions that must be properly mobilized at fertilization (Baumann & Walz 2001, Berridge 2002). It is well established that fertilization triggers an increase and oscillations in intracellular calcium concentration, resulting in the induction of CGE (Ducibella & Fissore 2008). The mechanisms of intracellular calcium release from the ER develop during oocyte maturation, and an ER cluster appears in the cortex of mature mouse ova (Mehlmann *et al.* 1995). Cortical reorganization of the ER occurs in many species before fertilization, and the presence of ER cortical clusters is thought to result in a high susceptibility of ova to initiate calcium oscillations following sperm entry (Ducibella & Fissore 2008). The sensitivity of the system to calcium release increases after maturation. A previous study reported differences

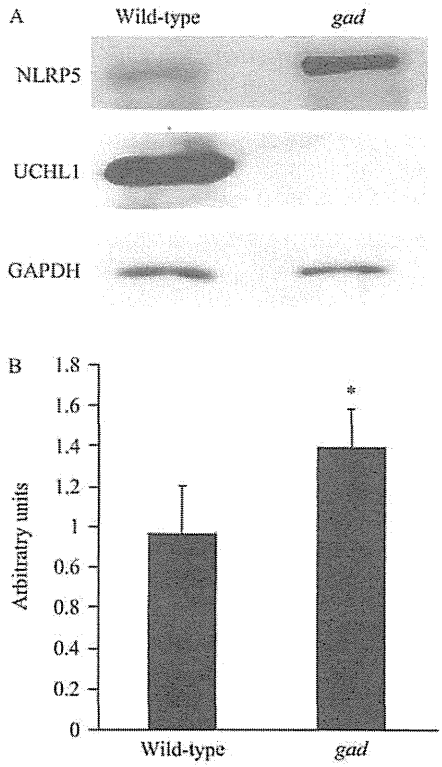

Figure 3 Expression of 'maternal antigen that embryos require' (NLRP5 (MATER)) and 'ubiquitin C-terminal hydrolase L1' (UCHL1) proteins in mouse ova. (A) Western blot analysis of NLRP5, UCHL1, and GAPDH in ova from wild-type ($n=5$) and *gad* ($n=4$) mice. UCHL1 was not detected in *gad* mouse ova. (B) NLRP5 protein levels in *gad* mouse ova were significantly higher than those in wild-type mice ($P=0.02$). Bars represent mean±s.d. Significant difference ($P<0.05$) is indicated by an asterisk.

regarding fertilization-induced calcium signals between immature oocytes and ova (Stricker 1999). Immature oocytes have less ER in the cortex compared with ovulated ova, and calcium release in response to fertilization is substantially less and slower than mature ova, resulting in polyspermy (Ducibella *et al.* 1993). Polyspermy in immature oocytes was attributed to complete failure or a CGE delay following calcium signaling (Ducibella *et al.* 1993). These findings suggest that polyspermy observed in *gad* mouse ova may have been caused by a delay in CGE resulting from its immaturity, although CGE and ZP react (Fig. 6). Furthermore, a recent study showed that calcium signaling plays a role in establishing the membrane block to polyspermy using ZP-free mouse ova (McAvey *et al.* 2002). Thus, *gad* mouse ova polyspermy was also considered to be due to the failure of the membrane block (Fig. 6). However, the mechanism for a polyspermy membrane block is largely unknown. Further examination is required to confirm this.

Additionally, we identified ER chaperones (ENPL, HSPA5, and CALR) by proteomic analysis, which were upregulated significantly in *gad* mouse ova. These chaperone proteins are constitutively expressed in the ER, and expression is regulated by the UPR, known as the ER signal transduction pathway (Rutkowski & Hegde 2010). Unfolded or malfolded proteins accumulating in the ER (ER stress) activate the UPR, which degrades the proteins via ER-associated degradation involving the ubiquitin–proteasome system (Yoshida 2007). Given that the ubiquitin–proteasome system is impaired due to the lack of UCHL1 in *gad* mouse ova, ER chaperones may be upregulated by the accumulation of abnormal proteins. Indeed, ER stress is induced by a UCHL1 inhibitor in neuronal cells (Tan *et al.* 2008). Thus, it is also possible that ER stress following an excess of abnormal protein causes ER dysfunction, and *gad* mouse ova showed an impaired polyspermy block (Fig. 6). However, further investigations are necessary to reveal the relationship between polyspermy and a UCHL1 deficiency in ova.

In conclusion, we identified UCHL1-related proteins by proteomic analysis using *gad* mouse ova. We also found that the NLRP5 protein level increased significantly in *gad* mouse ova vs wild-type mice. Furthermore, we observed that *gad* mouse ova contained less ER in the cortex. These results suggest that UCHL1 regulates the NLRP5 protein level in mouse ova maturation.

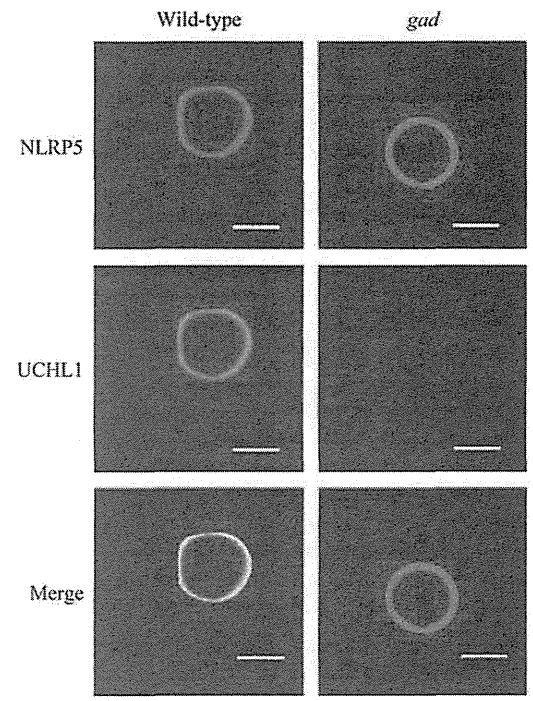

Figure 4 Localization of 'maternal antigen that embryos require' (NLRP5 (MATER)) and 'ubiquitin C-terminal hydrolase L1' (UCHL1) proteins in mouse ova. Immunocytochemical analysis of NLRP5 and UCHL1 in ova from wild-type and *gad* mice. NLRP5 immunoreactivity is seen on the plasma membrane of ova from wild-type and *gad* mice. NLRP5 and UCHL1 are co-localized on the plasma membrane of ova from wild-type mice. Bars, 50 μm.

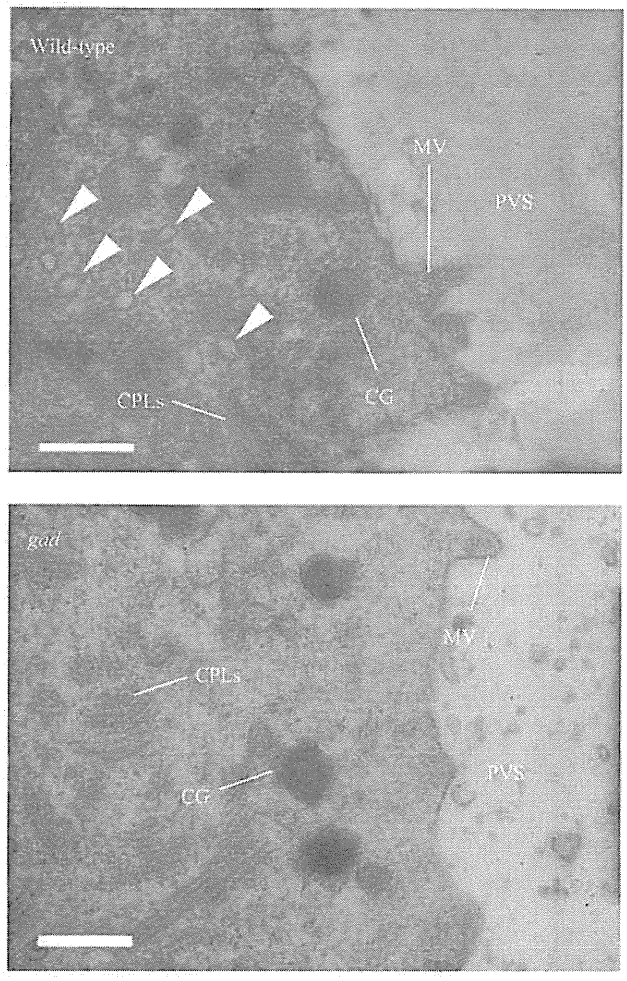

Figure 5 Ultrastructural study of ova from wild-type and *gad* mice by transmission electron microscopy. Basic cellular structures and cortical granule (CG), microvilli (MV), cytoplasmic lattices (CPLs), and perivitelline space (PVS) are observed in wild-type and *gad* mice. *gad* ova appear to have less endoplasmic reticulum (ER) than wild-type mice (arrowheads). Bars, 0.5 μm.

Materials and Methods

Animals

Nine-week-old BDF1 and *gad* female mice were used in this study. BDF1 mice were purchased from Nihon SLC, Inc. (Hamamatsu, Japan). The *gad* mouse is an autosomal recessive mutant obtained by cross-breeding CBA and RFM mice (Saigoh *et al.* 1999). The *gad* line is maintained at our institute. Genotyping was conducted using PCR with the following primers: F1, 5′-AGCTTGGAGCCTGTGGTTTCAACTC-3′; R1, 5′-TGGCAGCATCCTGAAAAGGAGAGAGGTG-3′; R2, 5′-TACAGATGGCCGTCCACGTTGTTGA-3′, as described elsewhere (Sakurai *et al.* 2008).

Animal care and handling were conducted in accordance with institutional regulations. These experiments were approved by the Animal Care and Use Committee of the Graduate School of Agricultural and Life Sciences, The University of Tokyo.

Ova collection

Female mice were superovulated with i.p. injections of 5 IU equine chorionic gonadotropin for 48 h, followed by 5 IU human chorionic gonadotropin (hCG). Ovulated ova were collected from the ampullae of the oviducts using the scratching method 15 h after hCG injection and placed in 400 μl droplets of HTF medium containing 0.4 mg/ml BSA. Then, 0.05% hyaluronidase was added to the medium to remove the cumulus cells.

Liquid chromatography–tandem mass spectrometry

The capillary reversed-phase μLC–MS/MS system (ZAPLOUS System, AMR, Inc., Tokyo, Japan) consisted of a Paradigm MS4 dual solvent delivery system (Michrom BioResources, Inc., Auburn, CA, USA) for HPLC, an HTC PAL autosampler (CTC Analytics, Zwingen, Switzerland), and Finnigan LTQ linear ion-trap mass spectrometers (ITMS, Thermo Fischer, San Jose, CA, USA) equipped with XYZ nanoelectrospray ionization (NSI) sources (AMR, Inc.). We used three wild-type mice and three *gad* mice for LC–MS/MS analysis and collected 20 ova from each mouse. Samples (20 ova each) were prepared using digestion solution to a final volume of 20 μl. Then, digested samples of 1.0 μl (equivalent to 1-ovum proteins) were automatically injected into a peptide L-trap column (Chem. Eval. Res. Inst., Saitama, Japan) on an injector valve for concentrating and desalting. Sample handling and injection were conducted with the HTC-PAL autosampler (CTC Analytics).

An injection volume was 1/20 equivalents. After desalting with 0.1% TFA (trifluoro acetic acid; aq.) containing 2% acetonitrile, the sample was loaded into a MAGIC C18 capillary reversed-phase column (3 μm, 200 Å, 150×0.2 mm i.d.; Michrom BioResources, Inc.) for separation. The mobile phase was as follows: A) 98% H_2O/2% CH_3CN/0.1% HCOOH and B) 10% H_2O/90% CH_3CN/0.1% HCOOH. The gradient conditions in the chromatographic run were as follows: B from 5% B (0 min) to 55% B (100 min), and then 95% B (1 min), 95% B (9 min), 5% B (1 min), and 5% B (9 min). Effluent at a flow rate of 0.5 ml/min was introduced into the mass spectrometer by the NSI interface via an injector valve with the L-trap column and the reversed phase (RP) column. The NSI needle (150/20 FortisTip; OmniSeparo-TJ, Hyogo, Japan), connected directly to the reverse-phase column outlet, was used as the NSI interface and the voltage was 2.0 kV, while the capillary was heated to 200 °C. No sheath or auxiliary gas was used.

Furthermore, the mass spectrometer was operated in a data-dependent acquisition mode in which MS acquisition with a mass range of 450–1800 m/z was automatically switched to MS/MS acquisition under the automated control of Xcalibur Software (Thermo Fisher, San Jose, CA, USA). The MS measurement sequence was Full MS (enhanced/profile), MS/MS (Top1: normal/centroid), MS/MS (Top2: normal/centroid), and MS/MS (Top3: normal/centroid). The parent ions were subjected to MS/MS scans with an isolation width of 2.0 m/z; the activation amplitude parameter was set at 35%. The trapping time was 50 ms under the auto gain control mode. Data were acquired using the dynamic mass exclusion windows that had an exclusion of 2.0 min duration and an exclusion mass width of −0.5 and +1.5 Da.

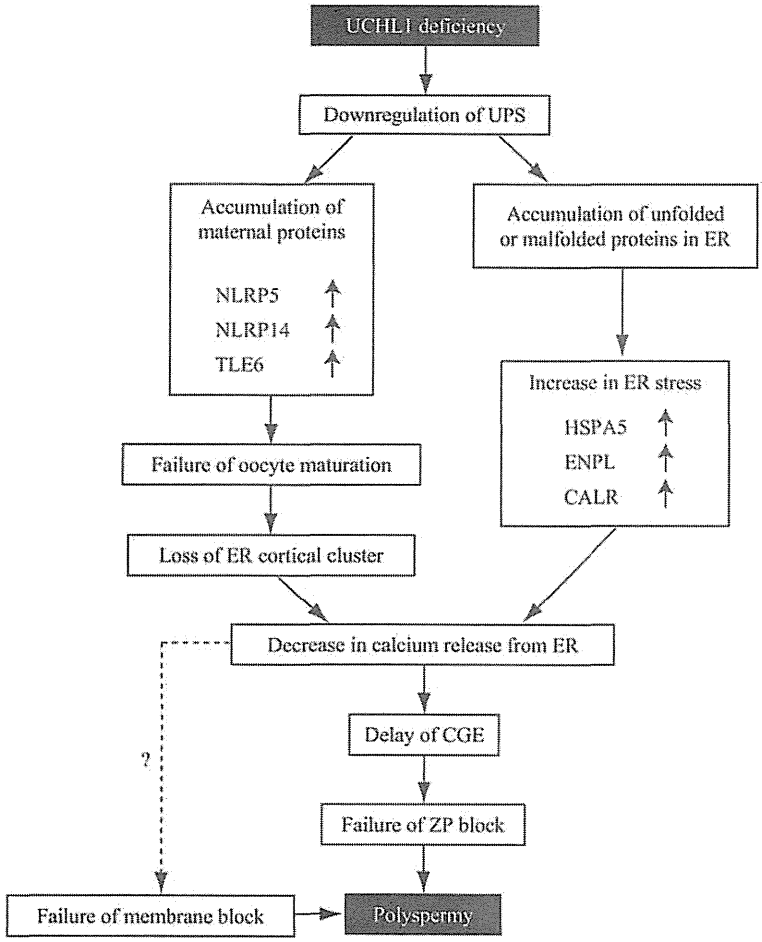

Figure 6 Consequences of UCHL1 deficiency in *gad* mouse ova. UCHL1 deficiency results in the downregulation of UPS and accumulation of maternal proteins in the cytoplasm and unfolded or malfolded proteins in the ER. These accumulations of protein in the cytoplasm and ER may contribute to the failure of oocyte maturation and increase in ER stress, which in turn decrease calcium release from the ER after fertilization. Thus, UCHL1 deficiency might downregulate CGE, ZP block, and membrane block and consequently induce polyspermy. UPS, ubiquitin–proteasome system; ER, endoplasmic reticulum; CGE, cortical granule exocytosis; ZP, zona pellucida.

Spectral analysis and database searching

All MS/MS data were investigated using the Bioworks (version 3.1; Thermo Fischer) against the NCBInr mouse (*Mus musculus*) database. The database searches allowed for variable modification of the methionine residue (oxidation, 116 Da), oxidation (M), peptide mass tolerance at 2.0 Da, and fragment mass tolerance at 1.0 Da. The identified proteins resulted from triplicate LC–MS runs for each sample and included one peptide identification. We performed label-free quantification on ovum proteins from *gad* mouse and wild-type mice (Kawamura *et al.* 2010).

Antibodies

Rabbit polyclonal anti-UCHL1 and UCHL3 antibodies were provided by Dr Kwon (Tyun-Puk University, South Korea). Mouse monoclonal anti-PGP9.5 antibody was obtained from Neuromics (Northfield, MN, USA). Rabbit polyclonal anti-cofilin and mouse monoclonal anti-GAPDH antibodies were purchased from Abcam. Rabbit anti-MATER antiserum was donated by the Laboratory of Cellular and Developmental Biology, NIDDK, National Institutes of Health (NIH), Bethesda, MD, USA.

Western blot analysis

Ova were subjected to SDS–PAGE using 8% gel for cofilin and 15% gel for NLRP5 proteins. The proteins were electrophoretically transferred to a PVDF membrane and blocked with 5% nonfat dried milk in PBS–Tween 80. The membranes were incubated individually with primary antibodies (cofilin, 1:10 000; MATER, 1:15 000; UCHL1, 1:10 000; and GAPDH, 1:10 000) at 4 °C overnight. Then, the membrane was incubated with primary antibody against GAPDH as an internal control for 1.5 h and further incubated with peroxidase-conjugated secondary antibody (goat antirabbit IgG, 1:10 000–15 000; goat antisheep IgG, 1:3000; and goat antimouse IgG, 1:10 000) for 1 h at room temperature. Immunoreactions were visualized by ECL plus (GE Healthcare Bio-Sciences, Piscataway, NJ, USA). Each immunoreactive band was quantified using Scion Image Software (NIH).

Phalloidin and immunohistochemical staining

For immunocytochemical staining, whole ova were fixed for 45 min with 4% paraformaldehyde in PBS and permeabilized for 20 min with 0.2% Triton X-100 in PBS. Nonspecific binding of immunoglobulins was blocked by incubating with Block

Ace for 45 min at room temperature. The sections were incubated with Alexa 488-phalloidin (1:2000) for 20 min at room temperature or with rabbit polyclonal anti-cofilin (1:10 000) antibody at 4 °C overnight. Then, they were further incubated with Alexa 488-conjugated anti-rabbit IgG for 1 h at room temperature.

For double-immunohistochemical staining, the sections were incubated with anti-MATER antiserum (1:10 000) and mouse monoclonal anti-UCHL1/PGP9.5 (1:40) antibody at 4 °C overnight. Then, they were further incubated with Alexa 488-conjugated anti-rabbit IgG and Alexa568-conjugated anti-mouse IgG for 1 h at room temperature. Stained sections were observed under a confocal laser microscope (Laser Scanning Microscope 510; Carl Zeiss, Oberkochen, Germany).

Transmission electron microscopy

Isolated ova were fixed in 2.5% glutaraldehyde/0.1 M phosphate buffer (PB) for 4 h at 4 °C. After washing with PBS, they were postfixed in 1% OsO_4 in 0.1 M PB for 2 h at 4 °C. They were then dehydrated and embedded in araldite M. Ultrathin sections were examined under a JEOL-1010 transmission electron microscope at 80 kV.

Statistical analyses

The mean and S.D. were calculated for all data. Student's *t*-test was used for all statistical analyses. A P value <0.05 was considered to indicate statistical significance.

Declaration of interest

The authors declare that there is no conflict of interest that could be perceived as prejudicing the impartiality of the research reported.

Funding

This study was supported by a grant-in-aid for scientific research from the Japan Society for the Promotion of Science.

Acknowledgements

We thank Takanori Nishimura and Kunihiko Naito for technical assistance. We also thank Dr Keiji Wada for providing *gad* mice, Dr Jungkee Kwon for providing the UCHL1 polyclonal antiserum, and Dr Jurrien Dean for providing the MATER polyclonal antiserum.

References

Bajoghli B 2007 Evolution of the *Groucho/Tle* gene family: gene organization and duplication events. *Development Genes and Evolution* **217** 613–618. (doi:10.1007/s00427-007-0167-y)

Baumann O & Walz B 2001 Endoplasmic reticulum of animal cells and its organization into structural and functional domains. *International Review of Cytology* **205** 149–214.

Beall S, Brenner C & Segars J 2010 Oocyte maturation failure: a syndrome of bad eggs. *Fertility and Sterility* **94** 2507–2513. (doi:10.1016/j.fertnstert.2010.02.037)

Berridge MJ 2002 The endoplasmic reticulum: a multifunctional signaling organelle. *Cell Calcium* **32** 235–249. (doi:10.1016/S014341600 2001823)

Buscarlet M & Stifani S 2007 The 'Marx' of Groucho on development and disease. *Trends in Cell Biology* **17** 353–361. (doi:10.1016/j.tcb.2007.07.002)

Carlier MF, Laurent V, Santolini J, Melki R, Didry D, Xia GX, Hong Y, Chua NH & Pantaloni D 1997 Actin depolymerizing factor (ADF/cofilin) enhances the rate of filament turnover: implication in actin-based motility. *Journal of Cell Biology* **136** 1307–1322. (doi:10.1083/jcb.136.6.1307)

Connors SA, Kanatsu-Shinohara M, Schultz RM & Kopf GS 1998 Involvement of the cytoskeleton in the movement of cortical granules during oocyte maturation, and cortical granule anchoring in mouse eggs. *Developmental Biology* **200** 103–115. (doi:10.1006/dbio.1998.8945)

DeRenzo C & Seydoux G 2004 A clean start: degradation of maternal proteins at the oocyte-to-embryo transition. *Trends in Cell Biology* **14** 420–426. (doi:10.1016/j.tcb.2004.07.005)

Ducibella T & Fissore R 2008 The roles of Ca^{2+}, downstream protein kinases, and oscillatory signaling in regulating fertilization and the activation of development. *Developmental Biology* **315** 257–279. (doi:10.1016/j.ydbio.2007.12.012)

Ducibella T, Kurasawa S, Duffy P, Kopf GS & Schultz RM 1993 Regulation of the polyspermy block in the mouse egg: maturation-dependent differences in cortical granule exocytosis and zona pellucida modifications induced by inositol 1,4,5-trisphosphate and an activator of protein kinase C. *Biology of Reproduction* **48** 1251–1257. (doi:10.1095/biolreprod48.6.1251)

Eletto D, Dersh D & Argon Y 2010 GRP94 in ER quality control and stress responses. *Seminars in Cell & Developmental Biology* **21** 479–485. (doi:10.1016/j.semcdb.2010.03.004)

Eliyahu E, Tsaadon A, Shtraizent N & Shalgi R 2005 The involvement of protein kinase C and actin filaments in cortical granule exocytosis in the rat. *Reproduction* **129** 161–170. (doi:10.1530/rep.1.00424)

Ellederova Z, Halada P, Man P, Kubelka M, Motlik J & Kovarova H 2004 Protein patterns of pig oocytes during *in vitro* maturation. *Biology of Reproduction* **71** 1533–1539. (doi:10.1095/biolreprod.104.030304)

Hatanaka Y, Nagai T, Tobita T & Nakano M 1992 Changes in the properties and composition of zona pellucida of pigs during fertilization *in vitro*. *Journal of Reproduction and Fertility* **95** 431–440. (doi:10.1530/jrf.0.0950431)

Huo LJ, Fan HY, Zhong ZS, Chen DY, Schatten H & Sun QY 2004 Ubiquitin–proteasome pathway modulates mouse oocyte meiotic maturation and fertilization via regulation of MAPK cascade and cyclin B1 degradation. *Mechanisms of Development* **121** 1275–1287. (doi:10.1016/j.mod.2004.05.007)

Kawamura T, Nomura M, Tojo H, Fujii K, Hamasaki H, Mikami S, Bando Y, Kato H & Nishimura T 2010 Proteomic analysis of laser-microdissected paraffin-embedded tissues: (1) stage-related protein candidates upon non-metastatic lung adenocarcinoma. *Journal of Proteomics* **73** 1089–1099. (doi:10.1016/j.jprot.2009.11.011)

Kim B, Kan R, Anguish L, Nelson LM & Coonrod SA 2010 Potential role for MATER in cytoplasmic lattice formation in murine oocytes. *PLoS ONE* **5** e12587. (doi:10.1371/journal.pone.0012587)

Kirkpatrick DS, Gerber SA & Gygi SP 2005 The absolute quantification strategy: a general procedure for the quantification of proteins and post-translational modifications. *Methods* **35** 265–273. (doi:10.1016/j.ymeth.2004.08.018)

Krone N, Hughes BA, Lavery GG, Stewart PM, Arlt W & Shackleton CH 2010 Gas chromatography/mass spectrometry (GC/MS) remains a pre-eminent discovery tool in clinical steroid investigations even in the era of fast liquid chromatography tandem mass spectrometry (LC/MS/MS). *Journal of Steroid Biochemistry and Molecular Biology* **121** 496–504.

Kruse U, Bantscheff M, Drewes G & Hopf C 2008 Chemical and pathway proteomics: powerful tools for oncology drug discovery and personalized health care. *Molecular and Cellular Proteomics* **7** 1887–1901.

Kwon J, Wang YL, Setsuie R, Sekiguchi S, Sato Y, Sakurai M, Noda M, Aoki S, Yoshikawa Y & Wada K 2004 Two closely related ubiquitin

C-terminal hydrolase isozymes function as reciprocal modulators of germ cell apoptosis in cryptorchid testis. *American Journal of Pathology* **165** 1367–1374. (doi:10.1016/S0002-9440(10)63394-9)

Kwon J, Mochida K, Wang YL, Sekiguchi S, Sankai T, Aoki S, Ogura A, Yoshikawa Y & Wada K 2005 Ubiquitin C-terminal hydrolase L-1 is essential for the early apoptotic wave of germinal cells and for sperm quality control during spermatogenesis. *Biology of Reproduction* **73** 29–35. (doi:10.1095/biolreprod.104.037077)

Li L, Baibakov B & Dean J 2008 A subcortical maternal complex essential for preimplantation mouse embryogenesis. *Developmental Cell* **15** 416–425. (doi:10.1016/j.devcel.2008.07.010)

Massicotte L, Coenen K, Mourot M & Sirard MA 2006 Maternal housekeeping proteins translated during bovine oocyte maturation and early embryo development. *Proteomics* **6** 3811–3820. (doi:10.1002/pmic.200500803)

McAvey BA, Wortzman GB, Williams CJ & Evans JP 2002 Involvement of calcium signaling and the actin cytoskeleton in the membrane block to polyspermy in mouse eggs. *Biology of Reproduction* **67** 1342–1352. (doi:10.1095/biolreprod67.4.1342)

Meberg PJ & Bamburg JR 2000 Increase in neurite outgrowth mediated by overexpression of actin depolymerizing factor. *Journal of Neuroscience* **20** 2459–2469.

Mehlmann LM, Terasaki M, Jaffe LA & Kline D 1995 Reorganization of the endoplasmic reticulum during meiotic maturation of the mouse oocyte. *Developmental Biology* **170** 607–615. (doi:10.1006/dbio.1995.1240)

Ohsugi M, Zheng P, Baibakov B, Li L & Dean J 2008 Maternally derived FILIA–MATER complex localizes asymmetrically in cleavage-stage mouse embryos. *Development* **135** 259–269. (doi:10.1242/dev.011445)

Osaka H, Wang YL, Takada K, Takizawa S, Setsuie R, Li H, Sato Y, Nishikawa K, Sun YJ, Sakurai M *et al.* 2003 Ubiquitin carboxy-terminal hydrolase L1 binds to and stabilizes monoubiquitin in neuron. *Human Molecular Genetics* **12** 1945–1958. (doi:10.1093/hmg/ddg211)

Pennetier S, Perreau C, Uzbekova S, Thelie A, Delaleu B, Mermillod P & Dalbies-Tran R 2006 MATER protein expression and intracellular localization throughout folliculogenesis and preimplantation embryo development in the bovine. *BMC Developmental Biology* **6** 26. (doi:10.1186/1471-213X-6-26)

Pfaffenbach KT & Lee AS 2011 The critical role of GRP78 in physiologic and pathologic stress. *Current Opinion in Cell Biology* **23** 150–156. (doi:10.1016/j.ceb.2010.09.007)

Qiu Y & Michalak M 2009 Transcriptional control of the calreticulin gene in health and disease. *International Journal of Biochemistry & Cell Biology* **41** 531–538. (doi:10.1016/j.biocel.2008.06.020)

Robert C, McGraw S, Massicotte L, Pravetoni M, Gandolfi F & Sirard MA 2002 Quantification of housekeeping transcript levels during the development of bovine preimplantation embryos. *Biology of Reproduction* **67** 1465–1472. (doi:10.1095/biolreprod.102.006320)

Rutkowski DT & Hegde RS 2010 Regulation of basal cellular physiology by the homeostatic unfolded protein response. *Journal of Cell Biology* **189** 783–794. (doi:10.1083/jcb.201003138)

Ryu KY, Sinnar SA, Reinholdt LG, Vaccari S, Hall S, Garcia MA, Zaitseva TS, Bouley DM, Boekelheide K, Handel MA *et al.* 2008 The mouse polyubiquitin gene *Ubb* is essential for meiotic progression. *Molecular and Cellular Biology* **28** 1136–1146. (doi:10.1128/MCB.01566-07)

Saigoh K, Wang YL, Suh JG, Yamanishi T, Sakai Y, Kiyosawa H, Harada T, Ichihara N, Wakana S, Kikuchi T *et al.* 1999 Intragenic deletion in the gene encoding ubiquitin carboxy-terminal hydrolase in gad mice. *Nature Genetics* **23** 47–51.

Sakurai M, Sekiguchi M, Zushida K, Yamada K, Nagamine S, Kabuta T & Wada K 2008 Reduction in memory in passive avoidance learning, exploratory behaviour and synaptic plasticity in mice with a spontaneous deletion in the ubiquitin C-terminal hydrolase L1 gene. *European Journal of Neuroscience* **27** 691–701. (doi:10.1111/j.1460-9568.2008.06047.x)

Sekiguchi S, Kwon J, Yoshida E, Hamasaki H, Ichinose S, Hideshima M, Kuraoka M, Takahashi A, Ishii Y, Kyuwa S *et al.* 2006 Localization of ubiquitin C-terminal hydrolase L1 in mouse ova and its function in the plasma membrane to block polyspermy. *American Journal of Pathology* **169** 1722–1729. (doi:10.2353/ajpath.2006.060301)

Stricker SA 1999 Comparative biology of calcium signaling during fertilization and egg activation in animals. *Developmental Biology* **211** 157–176. (doi:10.1006/dbio.1999.9340)

Su YQ, Sugiura K, Woo Y, Wigglesworth K, Kamdar S, Affourtit J & Eppig JJ 2007 Selective degradation of transcripts during meiotic maturation of mouse oocytes. *Developmental Biology* **302** 104–117. (doi:10.1016/j.ydbio.2006.09.008)

Sun QY 2003 Cellular and molecular mechanisms leading to cortical reaction and polyspermy block in mammalian eggs. *Microscopy Research and Technique* **61** 342–348. (doi:10.1002/jemt.10347)

Susor A, Ellederova Z, Jelinkova L, Halada P, Kavan D, Kubelka M & Kovarova H 2007 Proteomic analysis of porcine oocytes during *in vitro* maturation reveals essential role for the ubiquitin C-terminal hydrolase-L1. *Reproduction* **134** 559–568. (doi:10.1530/REP-07-0079)

Susor A, Liskova L, Toralova T, Pavlok A, Pivonkova K, Karabinova P, Lopatarova M, Sutovsky P & Kubelka M 2010 Role of ubiquitin C-terminal hydrolase-L1 in antipolyspermy defense of mammalian oocytes. *Biology of Reproduction* **82** 1151–1161. (doi:10.1095/biolreprod.109.081547)

Tan YY, Zhou HY, Wang ZQ & Chen SD 2008 Endoplasmic reticulum stress contributes to the cell death induced by UCH-L1 inhibitor. *Molecular and Cellular Biochemistry* **318** 109–115. (doi:10.1007/s11010-008-9862-x)

Tashiro F, Kanai-Azuma M, Miyazaki S, Kato M, Tanaka T, Toyoda S, Yamato E, Kawakami H, Miyazaki T & Miyazaki J 2010 Maternal-effect gene *Ces5/Ooep/Moep19/Floped* is essential for oocyte cytoplasmic lattice formation and embryonic development at the maternal–zygotic stage transition. *Genes to Cells* **15** 813–828. (doi:10.1111/j.1365-2443.2010.01420.x)

Tsaadon A, Eliyahu E, Shtraizent N & Shalgi R 2006 When a sperm meets an egg: block to polyspermy. *Molecular and Cellular Endocrinology* **252** 107–114. (doi:10.1016/j.mce.2006.03.037)

Wassarman PM & Litscher ES 2008 Mammalian fertilization: the egg's multifunctional zona pellucida. *International Journal of Developmental Biology* **52** 665–676. (doi:10.1387/ijdb.072524pw)

Wilkinson KD, Lee KM, Deshpande S, Duerksen-Hughes P, Boss JM & Pohl J 1989 The neuron-specific protein PGP 9.5 is a ubiquitin carboxyl-terminal hydrolase. *Science* **246** 670–673. (doi:10.1126/science.2530630)

Wilson PO, Barber PC, Hamid QA, Power BF, Dhillon AP, Rode J, Day IN, Thompson RJ & Polak JM 1988 The immunolocalization of protein gene product 9.5 using rabbit polyclonal and mouse monoclonal antibodies. *British Journal of Experimental Pathology* **69** 91–104.

Yoshida H 2007 ER stress and diseases. *FASEB Journal* **274** 630–658.

Zhang P, Dixon M, Zucchelli M, Hambiliki F, Levkov L, Hovatta O & Kere J 2008 Expression analysis of the *NLRP* gene family suggests a role in human preimplantation development. *PLoS ONE* **3** e2755. (doi:10.1371/journal.pone.0002755)

Zhang P, Ni X, Guo Y, Guo X, Wang Y, Zhou Z, Huo R & Sha J 2009 Proteomic-based identification of maternal proteins in mature mouse oocytes. *BMC Genomics* **10** 348. (doi:10.1186/1471-2164-10-348)

Received 19 April 2011
First decision 2 June 2011
Revised manuscript received 6 December 2011
Accepted 5 January 2012

Mucosal Adjuvanticity of Fibronectin-Binding Peptide (FBP) Fused with *Echinococcus multilocularis* Tetraspanin 3: Systemic and Local Antibody Responses

Zhisheng Dang[1,2], Jinchao Feng[1], Kinpei Yagi[3]*, Chihiro Sugimoto[4], Wei Li[5], Yuzaburo Oku[2]*

1 College of Life and Environmental Sciences, Minzu University of China, Beijing, People's Republic of China, 2 Parasitology Laboratory, School of Veterinary Medicine, Faculty of Agriculture, Tottori University, Tottori, Japan, 3 Department of Biological Science, Hokkaido Institute of Public Health, Sapporo, Japan, 4 Division of Collaboration and Education, Research Center for Zoonosis Control, Hokkaido University, Sapporo, Japan, 5 Qinghai Academy of Animal and Veterinary Medicine, Qinghai, People's Republic of China

Abstract

Background: Studies have shown that a bacterial fibronectin attachment protein (FAP) is able to stimulate strong systemic and mucosal antibody responses when it is used alone or co-administrated with other antigens (Ags). Thus, it has been suggested to be a promising adjuvant candidate for the development of efficient vaccines. However, the co-administered Ags and FAP were cloned, expressed and purified individually to date. In a recent study, we first evaluated the adjuvanticity of a fibronectin-binding peptide (FBP, 24 amino acids) of *Mycobacterium avium* FAP fused with *Echinococcus multilocularis* tetraspanin 3 (Em-TSP3) by detecting systemic and local antibody responses in intranasally (i.n.) immunized BALB/c mice.

Methodology/Principal Findings: Em-TSP3 and FBP fragments were linked with a GSGGSG linker and expressed as a single fusion protein (Em-TSP3-FBP) using the pBAD/Thio-TOPO expression vector. BALB/c mice were immunized i.n. with recombinant Em-TSP3-FBP (rEm-TSP3-FBP) and rEm-TSP3+CpG and the systemic and local antibody responses were detected by ELISA. The results showed that both rEm-TSP3-FBP and rEm-TSP3+CpG evoked strong serum IgG ($p<0.001$) and IgG1 responses ($p<0.001$), whereas only the latter induced a high level IgG2α production ($p<0.001$), compared to that of rEm-TSP3 alone without any adjuvant. There were no significant differences in IgG and IgG1 production between the groups. Low level of serum IgA and IgM were detected in both groups. The tendency of Th1 and Th2 cell immune responses were assessed via detecting the IgG1/IgG2α ratio after the second and third immunizations. The results indicated that i.n. immunization with rEm-TSP3-FBP resulted in an increased IgG1/IgG2α ratio (a Th2 tendency), while rEm-TSP3+CpG caused a rapid Th1 response that later shifted to a Th2 response. Immunization with rEm-TSP3-FBP provoked significantly stronger IgA antibody responses in intestine ($p<0.05$), lung ($p<0.001$) and spleen ($p<0.001$) compared to those by rEm-TSP3+CpG. Significantly high level IgA antibodies were detected in nasal cavity ($p<0.05$) and liver ($p<0.05$) samples from both groups when compared to rEm-TSP3 alone without any adjuvant, with no significant difference between them.

Conclusions: I.n. administration of rEm-TSP3-FBP can induce strong systemic and mucosal antibody responses in immunized BALB/c mice, suggesting that fusion of Em-TSP3 with FBP is a novel, prospective strategy for developing safe and efficient human mucosal vaccines against alveolar echinococcosis (AE).

Citation: Dang Z, Feng J, Yagi K, Sugimoto C, Li W, et al. (2012) Mucosal Adjuvanticity of Fibronectin-Binding Peptide (FBP) Fused with *Echinococcus multilocularis* Tetraspanin 3: Systemic and Local Antibody Responses. PLoS Negl Trop Dis 6(9): e1842. doi:10.1371/journal.pntd.0001842

Editor: David Joseph Diemert, The George Washington University Medical Center, United States of America

Received April 23, 2012; **Accepted** August 15, 2012; **Published** September 27, 2012

Funding: This work was financially supported by grants for Emerging and Re-emerging Infectious Diseases from the Ministry of Health, Labor and Welfare of Japan (H24-Shinko-ippann-006), Grant-in-Aid for Scientific research (C)#23580433 from the Ministry of Education, Culture, Sports, Science and Technology of Japan (MEXT) and JSPS KAKENHI Grant Number 24*02094. An academic communication between Minzu University of China was supported by "985 Research Projects" (CUN 985-03-03). The funders had no role in study design, data collection and analysis, decision to publish, or preparation of the manuscript.

Competing Interests: The authors have declared that no competing interests exist.

* E-mail: kinpei@iph.pref.hokkaido.jp (KY); oku@muses.tottori-u.ac.jp (YO)

Introduction

Echinococcus multilocularis infection in humans and rodents occurs after oncosphere-containing eggs are orally ingested. Oncospheres penetrate the mucosa of the small intestine and migrate via the hepatic vein to the liver where they form cyst masses and increasingly transform into multiple vesicles filled with fluid and protoscoleces. Only oncospheres hatching from eggs in the small intestine are able to transit the mucosa. Therefore, an effective echinococcosis vaccine must stimulate a local mucosal response to block both infection and disease development, as is the case for many micropathogens [1]. In addition, a systemic response is necessary to achieve protection against the spread of oncospheres. Parent vaccines are generally ineffective in stimulating mucosal immunity, whereas mucosally delivered immunogens trigger both local and systemic immune responses [1,2]. Administration of Ags with potent mucosal adjuvants is used to ensure that an efficient immune response is elicited. To data, only a few molecules have shown their potentials as mucosal adjuvants. However, their toxicity and potential side effects limited their use in human vaccination [3–7]. CpG oligodeoxynucleotides (ODN) has been proved to be an ideal mucosal adjuvant due to its non-toxicity and

Author Summary

Echinococcus metacestodes form a laminated layer and develop strategies to escape host immune responses once the infection established on the liver of intermediated host. One of the most important strategies is thought to be immunoregulation, where some molecules (e.g., antigen B) impair dendritic cell (DC) differentiation and polarize immature DC maturation towards a non-protective Th2 cell response. Therefore, it is more feasible to kill *Echinococcus* oncospheres in the early stage of infection in the intestine and blood. Systemic and local immune responses are believed to play a crucial role on oncosphere exclusion. Among antigen delivery systems, i.n. administration is the most efficient one, inducing both systemic and a full-range of mucosal immune responses. FAP is necessary to *M. avium* and *S. pyogenes* to efficiently attach and invade epithelial cells, and has been suggested as a potent vaccine adjuvant. Mucosal immune responses are induced after FAP binds to the fibronectin protein of host microfold (M) cells and DCs are activated. We developed a one-step delivery system where FAP and other Ags can be expressed, purified and immunized as one protein. The systemic and, in particular, the mucosal antibody responses induced by the fusion protein were detected to evaluate the adjuvanticity of FBP.

ability to induce strong systemic and/or local immune responses [8–12]. We recently showed that both systemic and local antibody responses were stimulated when CpG ODN was co-administered with rEm-TSP3 to BALB/c mice intranasally (i.n.). Unfortunately, they failed to induce a satisfied intestinal IgA response [13]; thus, this study focuses to find out other molecules as an adjuvant which may enhance intestinal IgA immune response.

Studies showed that the fibronectin-binding protein of *S. pyogenes* (SfbI) stimulates efficient, long-lasting serum and mucosal antibody responses against SfbI or other co-administered model Ags such as ovalbuin (OVA) and beta-galactosidase (beta-gal) [14–17]. The fibronectin-binding/attachment proteins of *S. pyogenes* (SfbI) and *M. avium* (FAP) are necessary for efficient attachment and invasion of epithelial cells by these microorganisms. After SfbI/FAP binds to the fibronectin protein on the surface of host M cells, DCs are activated and induce mucosal immune responses [18–20]. However, the use of FAP as an adjuvant for co-administration with other protective Ags requires separate cloning, expression and purification of each protein. To overcome this problem and develop a one-step delivery system, we cloned the linked fibronectin-binding peptide (FBP) of *M. avium* FAP and Em-TSP3 into a pBAD/Thio-TOPO expression plasmid. The identification of short FBP (72 bp) greatly facilitated this work [19,21,22], because it is easy to synthesize. In this study, the adjuvanticity of the fusion form of FBP and Em-TSP3 (rEm-TSP3-FBP) was evaluated by detecting systemic and mucosal antibody responses against Em-TSP3 vaccine.

Materials and Methods

Ethics statement

This study was carried out in strict accordance to the recommendations set out in the Guidelines for Animal Experimentation of the Japanese Association for Laboratory Animal Science and the protocol for the animal experiments was approved by the ethics committee of Hokkaido University (Permit Number: 09-0144) and the Hokkaido Institute of Public Health (Permit Number: K20-6). I.n. immunization and sacrification of mice were performed under isoflurane anesthesia and all efforts were made to minimize suffering.

Experimental animals

Fifteen five-week-old BALB/c mice (male) were divided into 5 groups and maintained in cages in a P3 animal room at 23–25°C with a 12 h light/dark cycle. Litter was cleaned weekly. They were provided with food and water *ad libitum*. Mice were immunized at 6 weeks of age.

Recombinant plasmid constructions

Em-TSP3-FAP recombinant plasmid construction was performed as previously described [23] and illustrated in Figure 1. The primers used for amplification of fragments were listed in Table 1. Briefly, FBP (peptide 265–288 of *M. avium paratuberculosis* FAP) was amplified by PCR with FBP-F/FBP-R primers and an *Xho*I restriction site and GSGGSG linker (nucleotide sequence: GGTAGCGGCGGTTCTGG T) introduced into FBP fragment by PCR with FBP-Linker$_{XhoI}$-F/FBP-Linker-R primers. The region encoding the LEL (larger extracellular loop) domain of Em-TSP3 was amplified from the full-length enriched cDNA library of *E. multilocularis* larvae. The GSGGSG linker, *Hind*III and *Xho*I restriction sites were introduced into Em-TSP3 fragment by PCR with TSP3$_{HindIII}$-F/TSP3$_{XhoI}$-Linker-R primers. These two reconstructed fragments were combined by fusion PCR with TSP3$_{HindIII}$-F/FBP-Linker-R primers. The combined Em-TSP3-FBP fragment was then subcloned into pBAD/Thio-TOPO expression vector (Invitrogen, USA). Gene TaqNT polymerase (Nippon Gene, Japan) was used in PCR reaction.

Protein expression and purification

Recombinant protein expression and purification was performed as previously described [23]. Briefly, *Escherichia coli* TOP10 cells (Invitrogen, USA) were transformed with recombinant plasmid according to the manufacturer's instructions (pBAD/TOPO-ThioFusion Expression Kit, Invitrogen, USA). Recombinant protein from *E. coli* lysates was purified with a HisTrap affinity column (HisTrap FF crude 1 ml, GE Healthcare, USA) under non-denaturing conditions and stored at −80°C. rEm-TSP3 alone was also expressed, purified and used as the antigen in ELISA instead of rEm-TSP3-FBP, to deplete the reaction caused by FBP peptide.

Hydrophobicity plot prediction and tertiary structure analysis of expressed proteins

To confirm the solubility of rEm-TSP pre- and post-fusion with FBP, hydrophobicity plot was predicted by the Kyte–Doolittle hydropathy plot program (http://fasta.bioch.virginia.edu/fasta_www2/fasta_www.cgi?rm = misc1). The amino acid sequence of Em-TSP3 was aligned with protein sequences in the structural database using the Phyre (Protein Homology/analogy Recognition Engine) server at Imperial College (http://www.sbg.bio.ic.ac.uk/phyre/) [24] and the 3-dimensional structure was further activated.

Immunization of mice and sample collection

BALB/c mice (3 per group) were immunized i.n. three times with PBS, PBS+CpG, rEm-TSP3, rEm-TSP3+CpG and rEm-TSP3-FBP on a weekly basis. A dose of 50 μg per mouse (in 50 μl PBS) was used for three immunizations. This is independently reported here because this work was focused on evaluating the adjuvanticity of FBP as a novel strategy for vaccine development. CpG OND data is cited here to show the

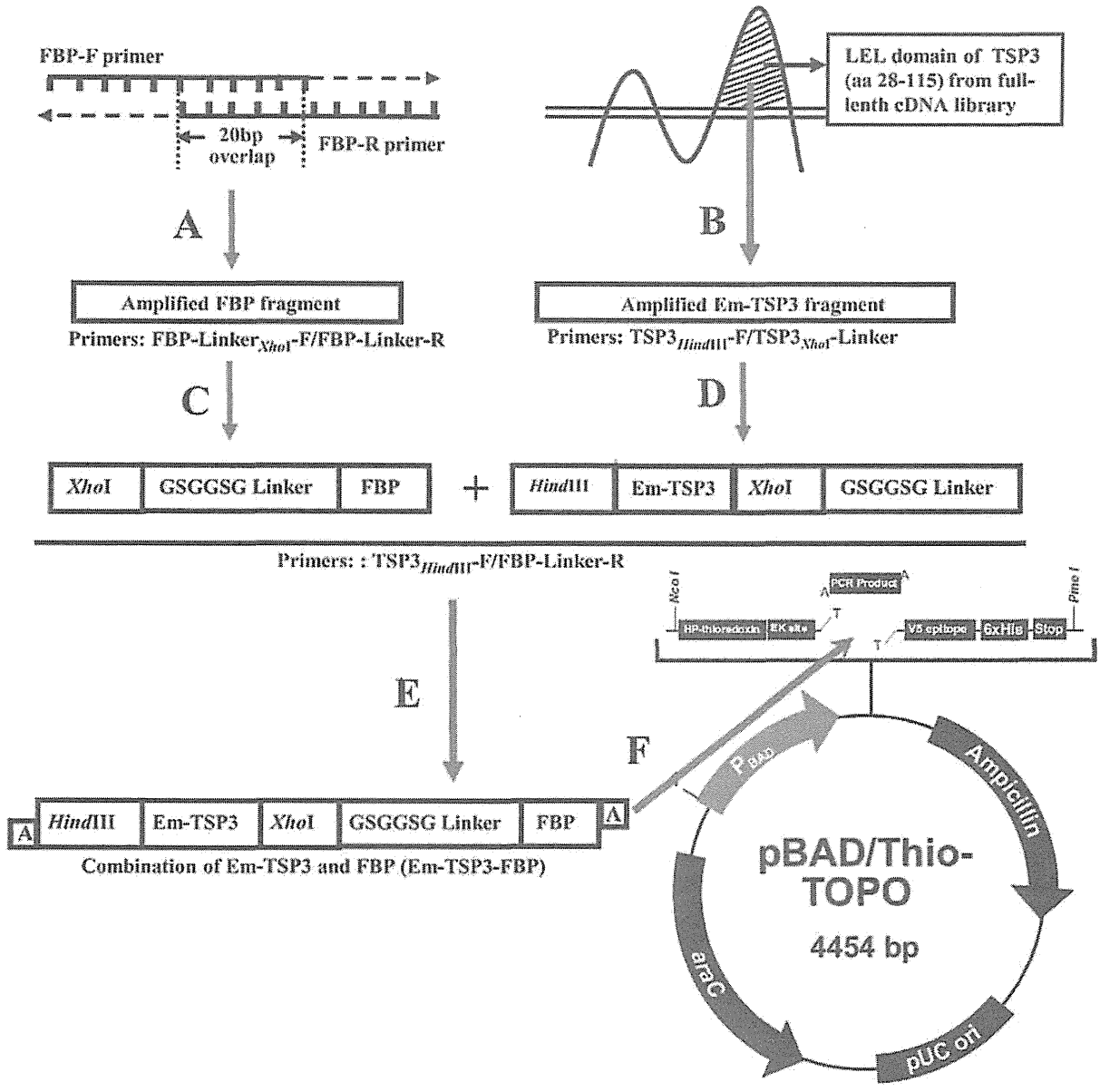

Figure 1. Schematic illustration of construction of fusion rEm-TSP3-FBP plasmid. (A) Synthesis of FBP. (B) Amplification of Em-TSP3 LEL from full-length cDNA library. (C) Ligation of linker to FBP fragment. (D) Ligation of linker to Em-TSP3 fragment. (E) Combination of FBP and Em-TSP3 (Em-TSP3-FBP) by fusion PCR. (F) Insertion of Em-TSP3-FBP into pBAD/Thio-TOPO cloning and expression vector.
doi:10.1371/journal.pntd.0001842.g001

adjuvanticity of FBP under the same experiment conditions [13]. A dose of 1 nM CpG ODN (Hokkaido System Science, Japan) was used per mouse. Retro-orbital blood collection was performed on mice one week after the second and third immunizations using glass capillary pipettes (Hirschmann, Germany) and the serum was isolated. Mice from each group were sacrificed one week after the third immunization and the nasal cavity washes, intestine, liver, lung and spleen were collected in 500 µl of PBS (pH 7.4). A 10-cm fragment of the ileal region was excised and the intestinal tube was opened and immersed in 250 µl of PBS; liver, lung and spleen were homogenized in 500 µl of PBS separately and vigorously vortexed, followed by centrifugation to remove insoluble debris. The sera and collected supernatants were stored at −20°C for further use.

Detection of systemic and local antibody responses by ELISA

Indirect ELISA was conducted for the antibody analysis as previously described [23]. Briefly, 96-well microtiter plates (Corning, USA) were coated with rEm-TSP3 protein (0.25 µg/well), blocked with 5% skim milk. For serum IgG, IgG1, IgG2α, IgA and IgM detection, plates were incubated with sera at a dilution of 1: 2,000 followed by incubation with horseradish

Table 1. List of primers used for fragments amplification.

Fragment (bp)	Primers	Sequence of primers	Tm (°C)
FBP (72)	FBP-F	5′GGCAACGCGCAACGCTGGTTCGTCGTCTGGCTGGGCACCTCGAACG3′	60
	FBP-R	5′CTTGGCCGCGACCTTGTCCACCGGGTCGTTCGAGGTGCCCAGCCAG3′	
FBP-Linker (96)	FBP-Linker$_{XhoI}$-F	5′*CTCGAG*GGTAGCGGCGGTTCTGGTGGCAACGCGCAACGCTGG3′	60
	FBP-Linker-R	5′TTACTTGGCCGCGACCTTGTCCA3′	
TSP3-Linker (294)	TSP3$_{HindIII}$-F	5′*AAGCTT*ATTCCTGATAACCTAAACAAAGCAG3′	55
	TSP$_{XhoI}$-linker-R	5′GAACCGCCGCTACC*CTCGAG*GAGG GTTTTGTTCTCTGCCA3′	
TSP3-FBP (366)	TSP3$_{HindIII}$-F	5′*AAGCTT*ATTCCTGATAACCTAAACAAAGCAG3′	60
	FBP-Linker-R	5′TTACTTGGCCGCGACCTTGTCCA3′	

F = forward;
R = reverse;
Tm = melting temperature.
doi:10.1371/journal.pntd.0001842.t001

peroxidase (HRP)-conjugated anti-mouse IgG (Invitrogen, USA), IgG1 (Rockland, USA), IgG2α (Southern Biotech, USA), IgA (Invitrogen, USA) and IgM (MP Biomedicals, USA). For IgA antibody detection in nasal cavity, intestine and liver, plate were incubated with nasal cavity washes, intestine washes, liver, lung and spleen extracts at a dilution of 1: 10, respectively, followed by incubation with HRP-conjugated anti-mouse IgA. A color reaction was developed by the addition of 100 µl of TMB (3, 3′, 5, 5′-tetramethylbenzidine) substrate (Dojindo, Japan). Absorbance was measured at 450 nm on a Biotrak II plate reader (Amersham Biosciences, USA).

Statistical analyses

Data was analyzed using one-way ANOVA followed by a multiple comparison Tukey's test. Differences were considered statistically significant at $p<0.05$, very significant at $p<0.01$ and extremely significant at $p<0.001$.

Results

Amplification of Em-TSP3-FBP fragment by fusion PCR

Em-TSP3 (276 bp including *Xho*I, *Hind*III sites) and FBP (72 bp) were amplified separately and linked with GSGGSG

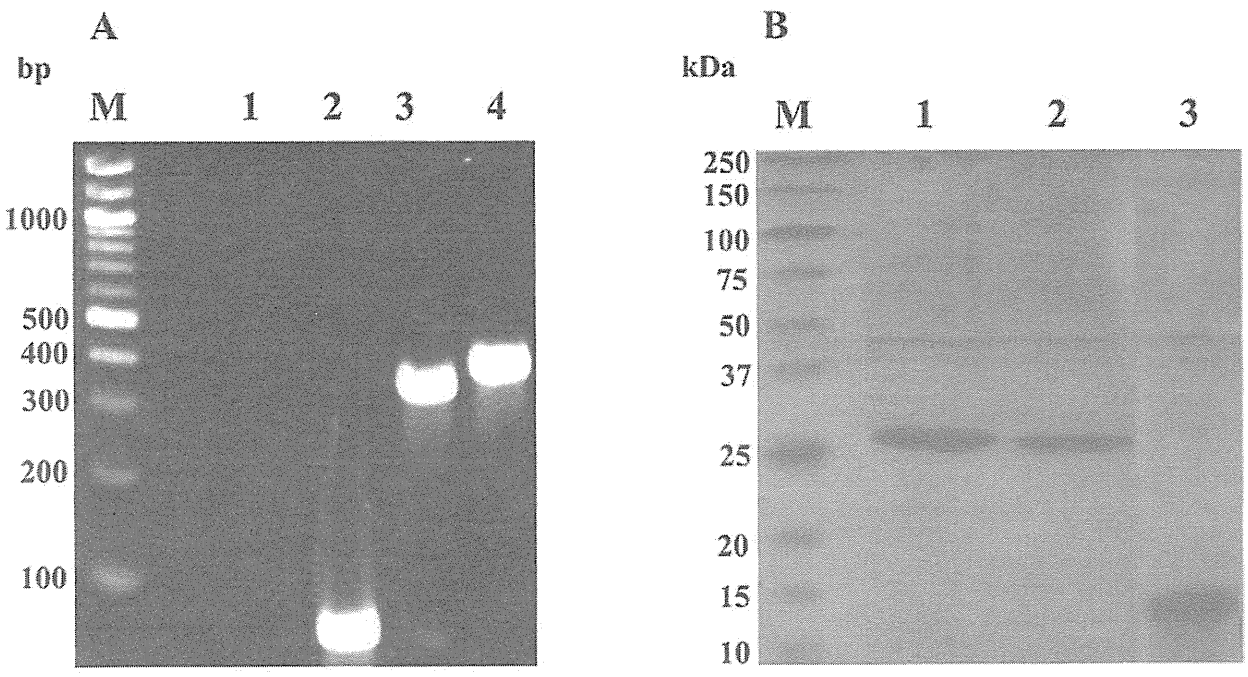

Figure 2. Cloning and expression of recombinant Em-TSP3-FBP protein. (A) Synthesis of FBP and Cloning of the LEL and Em-TSP3-FBP. M, marker. Lane 1. Negative control (H_2O). Lane 2. Synthesized FBP (72 bp). Lane 3. PCR product of Em-TSP3 LEL (276 bp). Lane 4. PCR product of Em-TSP3-FBP (366 bp). (B) Expression of recombinant Em-TSP3-FBP (fused with thioredoxin (TRX)). SDS-PAGE gel stained with Coomassie Blue showing purified rEm-TSP3 (Lane 1, 26.2 kDa), Em-TSP3-FBP (Lane 2, 29.3 kDa) and control TRX (Lane 3, 16 kDa). M, the molecular weight marker.
doi:10.1371/journal.pntd.0001842.g002

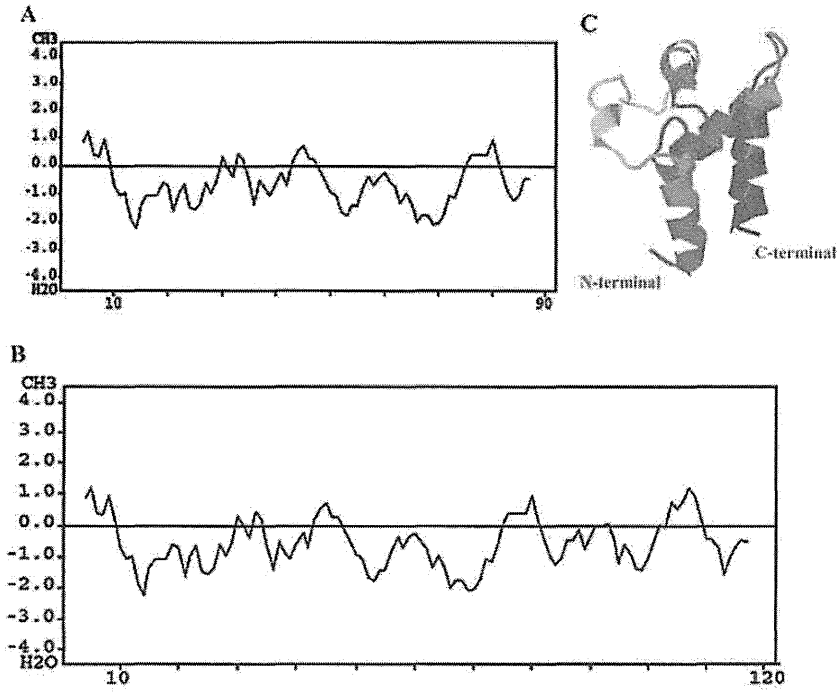

Figure 3. Solubility and 3-D structure of expressed proteins. Comparison of hydropathy plots of Em-TSP3 (A) and Em-TSP3-FBP (B). Hydropathy plots of the predicted amino acid sequences were obtained using the Kyte-Doolittle hydropathy plot program (http://fasta.bioch.virginia.edu/fasta_www2/fasta_www.cgi?rm=misc1). Hydrophobic residues are positive. (C) 3-D structure prediction of Em-TSP3 LEL domain. The amino acid sequence of Em-TSP3 (LEL) was aligned with protein sequences in the structural database using the Phyre (Protein Homology/analogy Recognition Engine) server at Imperial College (http://www.sbg.bio.ic.ac.uk/phyre/). The three-dimensional structure was further activated.
doi:10.1371/journal.pntd.0001842.g003

linker (18 bp) by fusion PCR. A band of 366 bp was observed in the agarose gel under ultraviolet light (Figure 2A).

Expression of fusion rEm-TSP3-FBP protein

SDS-PAGE analysis showed that Em-TSP3 at approximately 26 kDa of and Em-TSP3-FBP at 29 kDa were expressed as predicted (Figure 2B).

Solubility and 3-D structure of expressed proteins

The hydrophobicity plot prediction showed that after the fusion of Em-TSP3 and FBP, there was no significant change in solubility compared to Em-TSP3 alone (Figure 3A,3B). The 3-dimensional structure illustration of Em-TSP3 showed that the C-terminal is exposed outside (Figure 3C).

Serum antibody responses

Systemic antibody responses against rEm-TSP3+CpG and rEm-TSP3-FBP evoked by i.n. administrations were detected by ELISA. Compared to PBS control or Em-TSP3 alone, significant serum IgG ($p<0.001$) (Figure 4A) and IgG1 ($p<0.001$) (Figure 4B) antibody responses were detected in both the rEm-TSP3+CpG and rEm-TSP3-FBP groups ($p<0.001$). Only the former protein induced a significantly higher IgG2α response ($p<0.001$) (Figure 4C). No significant differences were observed between these two groups in IgG and IgG1 production. Very low level serum IgM (Figure 4D) and IgA antibodies (Figure 4E) were detected, with a significant difference in IgM production ($p<0.001$) between the groups (Figure 4D). There were no significant serum antibody responses to rEm-TSP3 alone (Figure 4A–4D).

The Th1 and Th2 cell responses were assessed via IgG1/IgG2α ratio (Table 2). Two weeks post-immunization, a predominantly Th1 response was detected in mice immunized with rEm-TSP3+CpG, but the IgG1/IgG2α ratio dramatically reduced at 3 weeks post-immunization (a Th2 tendency). Conversely, immunization with rEm-TSP3-FBP resulted in a Th2-predominated response.

Mucosal antibody responses

Very strong IgA responses ($p<0.001$) were detected in the nasal cavity samples from both the rEm-TSP3+CpG and rEm-TSP3-FBP groups ($p<0.001$), with no significant difference between them (Figure 5A). Significant IgA responses were detected in intestinal samples ($p<0.001$) from both groups, with the rEm-TSP3-FBP group being significantly higher ($p<0.05$) (Figure 5B). High liver IgA antibody levels were also detected in both groups ($p<0.001$), with no significant difference between them (Figure 5C). Significantly stronger IgA antibody responses were found in lung and spleen of both rEm-TSP3+CpG and rEm-TSP3-FBP groups ($p<0.001$). There was a clear difference between the groups, with the latter being extremely higher (Figure 5D,5E) ($p<0.001$). No significant IgA antibody responses were detected in any tissues of other control groups (Figure 5). Figure S1 shows the potential mechanism whereby Em-TSP3 induces strong mucosal antibody responses enhanced by fused FBP of *M. avium* FAP.

Discussion

We have previously shown that i.n. vaccination of rEm-TSP3 with CpG ODN adjuvant induces strong systemic and local

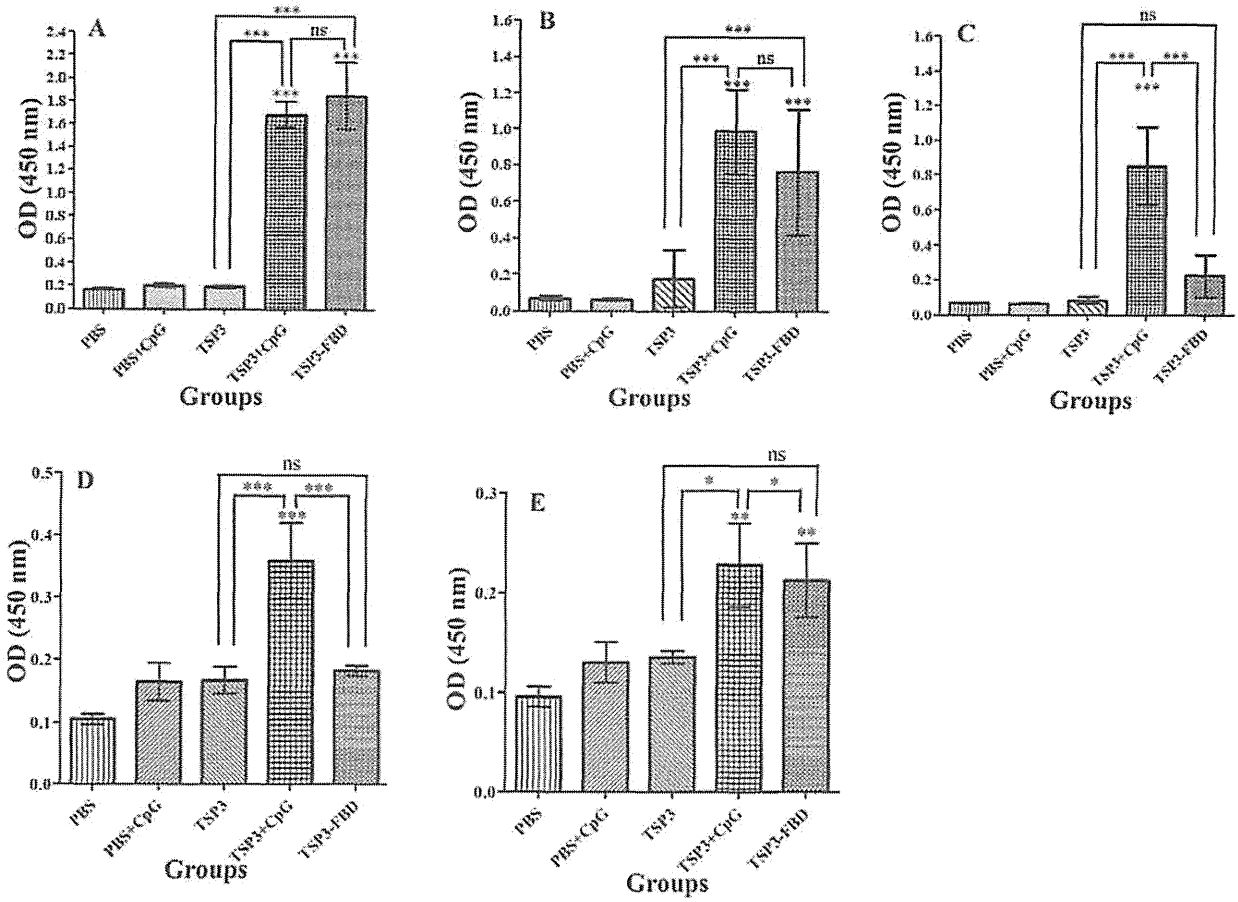

Figure 4. ELISA detection of serum antibody responses. Serum antibody responses were detected in BALB/c mice immunized with rEm-TSP3+CpG or rEm-TSP3-FBP intranasally after the third immunization. Absorbance (OD value at 450 nm) of sera IgG (A), IgG1 (B), IgG2α (C), IgM (D) and IgA (E) were presented in different bars. The S.D. is indicated by vertical lines. Significant differences between the vaccinated groups and the PBS control group are denoted by an asterisk over the bar. Significant differences between any of two groups are denoted by an asterisk over the line connecting them. n = 3 per group; *$p<0.05$ (significant); **$p<0.01$ (very significant); ***$p<0.001$ (extremely significant).
doi:10.1371/journal.pntd.0001842.g004

antibody responses with a >60% reduction in cyst lesion number reduction (CLNR) in the liver of BABL/c mice [13]. CpG DNA contains unmethylated CpG motifs (often given in the form of synthetic oligodeoxynucleotides (CpG ODN)), which contributes to its adjuvant activities by stimulating B cells [25] and activating DCs [26]. As a novel adjuvant, CpG OND induces Th1-like responses [27,28]. CpG ODN has recently been shown to act as potent adjuvants for vaccines delivered by i.n. inhalation [29–31]. However, in our previous study it didn't induce satisfied intestinal IgA production [13]. Because the nature infection of AE is closely associated to gastrointestinal tract, intestinal IgA is thought to be the first lines of defences against early infection by *E. multilocularis* [32]. We evaluated the efficiency of potent molecules such as FAPs to act as an adjuvant and enhanced mucosal IgA antibody responses.

Table 2. Th1/Th2 tendency post-the third immunization with rEm-TSP3+CpG and rEm-TSP3-FBP.

Protein	Weeks p.i.	IgG1*	IgG2α*	IgG1/IgG2α ratio
rEm-TSP3+CpG	2 weeks p.i.	0.344±0.098	0.432±0.148	0.80
	3 weeks p.i.	1.014±0.233	0.834±0.201	1.22
rEm-TSP3-FBP	2 weeks p.i.	0.214±0.110	0.148±0.099	1.446
	3 weeks p.i.	0.667±0.347	0.225±0.108	2.964

i.n. = intranasal;
p.i. = post-immunization;
*Values are presented as means ± standard deviation.
doi:10.1371/journal.pntd.0001842.t002

FAPs are a family of fibronectin-binding proteins that are present in several species of bacteria [22]. The attachment and internalization of *Mycobacterium* by epithelial cells were shown to be dependent on the interaction between FAPs and fibronectin [19,21,23,33]. Moreover, after targeting and invasion of host M cells by *Mycobacterium* by the formation of a fibronectin bridge between *Mycobacterium* FAP and integrins on host M cells [20], FAP modulates adaptive immune responses by inducing maturation and activation of DCs, driving a predominantly Th1 polarization [34].

We are the first to create a vector containing the fusion form of *M. avium paratuberculosis* FBP and Em-TSP3. Em-TSP3 and FBP were linked with a GSGGSG linker, which is a commonly used